


Gravitational lensing in the charged NUT–de Sitter spacetime

Torben C. Frost^{*}

ZARM, University of Bremen, 28359 Bremen, Germany and Institute for Theoretical Physics,
Leibniz University Hannover, 30167 Hannover, Germany

 (Received 28 December 2021; accepted 22 February 2022; published 30 March 2022)

It is a long-standing open question if a gravitomagnetic charge, the gravitational analogon to a hypothetical magnetic charge in electrodynamics, exists in nature. It naturally occurs in certain exact solutions to Einstein’s electrovacuum-field equations with cosmological constant. The charged NUT–de Sitter metric is such a solution. It describes a black hole with electric and gravitomagnetic charges and a cosmological constant. In this paper we will address the question how we can observe the gravitomagnetic charge using gravitational lensing. For this purpose we first solve the equations of motion for lightlike geodesics using Legendre’s canonical forms of the elliptic integrals and Jacobi’s elliptic functions. We fix a stationary observer in the domain of outer communication and introduce an orthonormal tetrad. The orthonormal tetrad relates the direction under which the observer detects a light ray to its latitude-longitude coordinates on the observer’s celestial sphere. In this parametrization we rederive the angular radius of the shadow, formulate a lens map, discuss the redshift, and the travel time. We also discuss relevant differences with respect to spherically symmetric and static spacetimes and how we can use them to determine if an astrophysical black hole has a gravitomagnetic charge.

DOI: [10.1103/PhysRevD.105.064064](https://doi.org/10.1103/PhysRevD.105.064064)

I. INTRODUCTION

The charged NUT–de Sitter metric belongs to the more exotic solutions of Einstein’s electrovacuum-field equations with cosmological constant. It is axisymmetric and stationary and belongs to the Plebański-Demiański family of spacetimes of Petrov type D [1]. In addition to the mass parameter m , the electric charge e and the cosmological constant Λ it contains two parameters n and C . In analogy to a hypothetical magnetic monopole with magnetic charge b the parameter n is usually referred to as “gravitomagnetic charge.” The parameter C is called the Manko-Ruiz parameter [2]. The spacetime is usually interpreted to describe a black hole; however, unlike the Reissner-Nordström–de Sitter metric it does not contain a curvature singularity at $r = 0$. The original Taub-NUT spacetime was discovered in two steps. First the time-dependent part of the spacetime was discovered by Taub in 1951 [3]. In 1963 Newman *et al.* [4] used the Newman-Penrose formalism to derive three different metrics characterized by geodesic rays which do not diverge or shear but curl. One of these metrics they identified as a generalization of the Schwarzschild metric, the so-called NUT metric. Newman *et al.*, and about one month later Misner [5], also pointed out that Taub’s solution can be interpreted as an extension of their spacetime. Misner [5] was also the first who referred to the spacetime as “NUT

space.” In its original form the spacetime is asymptotically flat in the sense that for $r \rightarrow \infty$ the Riemann tensor vanishes. However, the spacetime does not become asymptotically Minkowskian [5]. Misner also noted that either the metric or the time coordinate t has a singularity at $\vartheta = \pi$ (for this historical reason the axial singularities are called Misner strings). Bonnor [6] investigated the nature of this singularity and came to the conclusion that it can be interpreted as a semi-infinite massless rotating rod that serves as a source of angular momentum (see also the work of Sackfield [7]). He also pointed out that the strength of the Misner string is directly related to the gravitomagnetic charge n . The parameter C is also closely tied to the axial singularities. It was introduced by Manko and Ruiz [2] and can be used to control the number (one or two) and location of the axial singularities. Analogously to the Schwarzschild metric the NUT metric can also be generalized. According to Griffiths and Podolský [8] the NUT metric with electric charge was first discovered by Brill [9] (note that with a sufficiently large electric charge e the charged NUT metric can also be interpreted as a wormhole, see, e.g., Clément *et al.* [10]) and the charged NUT–de Sitter metric was discovered in 1972 by Ruban [11]. The charged NUT–de Sitter metrics (whenever we use the plural we will refer to the whole family of metrics with gravitomagnetic charge in the following) are interesting from the physical perspective because they represent exact solutions to Einstein’s electrovacuum-field equations with cosmological constant which in addition to the mass parameter m also incorporate a

^{*}torben.frost@zarm.uni-bremen.de

gravitomagnetic mass n (to maintain consistency throughout the paper hereafter we will continue to refer to it as gravitomagnetic charge). However, the presence of the Misner strings leads to two undesirable aspects. First, although the Misner strings are massless it is unclear if geodesics can be continued through the axes. While many authors advocate that the spacetime is geodesically incomplete, see, e.g., the work in [12–14], Clément *et al.* [15] investigated this aspect for the NUT metric and came to the conclusion that geodesics can be smoothly continued through the Misner strings (we will see that for the spatial coordinates this argument can also be transferred to all charged NUT–de Sitter metrics). The second problematic aspect of the NUT metric is that close to the Misner strings it contains regions with closed timelike curves. Misner [5] demonstrated that the axial singularities can be removed by introducing a periodic time coordinate; however, this step does not alleviate the problem but actually makes it worse. Using the periodic time coordinate the spacetime contains closed timelike curves everywhere, which is even less desirable. The presence of closed timelike curves makes the spacetime on the first view appear unphysical; however, the presence of closed timelike curves is limited to a narrow region around the Misner strings. Thus the NUT metric may still serve as an approximate model for a spacetime with gravitomagnetism as long as these regions are excluded.

In astrophysical settings the gravitomagnetic charge is expected to be very small [16,17]. Therefore, if we ever want to have a chance to detect visible effects caused by the gravitomagnetic charge we need gravitationally heavy objects. Supermassive black holes (SMBHs) at the center of galaxies are ideal candidates for such objects. Because we are currently not able to send any probes to SMBHs we have to rely on information carried to us by electromagnetic or gravitational radiation. Present-day gravitational wave detectors such as Laser Interferometer Gravitational Wave Observatory (LIGO) [18], Virgo [19], and KAGRA [20] so far only detected gravitational waves from stellar mass binary black hole and neutron star mergers and thus even with very high accuracy gravitational wave templates it is very likely that imprints of the gravitomagnetic charge on the detected gravitational wave signals are impossible to resolve. On the other hand recent technological advances in Very Large Baseline Interferometry (VLBI) lead to the observation of the shadow of the supermassive black hole in the galaxy M87 by the Event Horizon Telescope (EHT) [21]. The EHT has an angular resolution of about $25 \mu\text{as}$ at a wavelength of 1.3 mm [22]. This resolution is high enough to demonstrate that M87 contains an object that casts a shadow; however, the shape of the shadow is strongly blurred by the surrounding accretion disk and thus without further information its exact shape is difficult to reconstruct from observations alone. Because the resolution of ground-based VLBI is limited by the distribution

of radio telescopes on the surface of Earth we can only enhance it by extending VLBI to space. Space VLBI reaches back to the late 1970s. The most recent space VLBI program used the Spektr-R satellite [23,24] as spaceborne station and was terminated in 2019. The antenna of Spektr-R was able to observe at four wavelengths between 1 and 100 cm and thus did not operate in the millimeter/submillimeter range required for VLBI observations of supermassive black holes. Satellite missions attempting to achieve observations at these wavelengths are currently in their planning stage and will allow enhanced observations of the shadow in M87 and, potentially, also the observation of the centers of more distant galaxies. Therefore, from today’s perspective observing light gravitationally lensed by SMBHs promises the best chance to detect effects caused by the presence of the gravitomagnetic charge n .

Gravitational lensing in the weak- and strong-field regimes of the NUT metric has already been investigated by several authors. Gravitational lensing in the NUT metric was first investigated by Zimmerman and Shahir in 1989 [25]. They first showed that in the NUT metric all geodesics lie on spatial cones and then calculated the bending angle up to the first nonvanishing order in n for light rays on these cones. Up to first order in m their result was independently reproduced by Lynden-Bell and Nouri-Zonoz [16]. In addition Lynden-Bell and Nouri-Zonoz defined a simple lens map. They determined area magnification and the axial ratio of the image of a small circular source. In [26] Nouri-Zonoz and Lynden-Bell present a more thorough analytical approach to gravitational lensing in the NUT metric. After first rederiving the light-bending formula on a cone the authors proceed to define a different version of the lens equation and the magnification factor. In addition, they derive the geometric time delay and the Shapiro time delay between two images of the same source. Both works showed that the presence of a gravitomagnetic charge is associated with a twist in the observed lensing pattern. In [17] Rahvar and Nouri-Zonoz used these results to investigate gravitational microlensing in the NUT metric. While in all previous works the deflection angle was calculated using a simple expansion, Halla and Perlick [27] used a different approach. Following the work of Werner [28] they used the Gauss-Bonnet theorem to derive the deflection angle. The strong-field deflection limit was first investigated by Wei *et al.* [29] for Kerr–NUT spacetimes. Using numerical and analytical methods the authors constructed a lens equation for light rays in and close to the equatorial plane. In addition they derived the critical curves and the caustic structure, and the magnification of the images near the caustic points. Sharif and Iftikhar [30] investigated strong gravitational lensing in the equatorial plane of accelerating Kerr–NUT black holes. Finally, Grenzbach *et al.* [31,32] investigated the photon region and the shadow of Kerr–Newman–NUT black holes with cosmological constant. While all these works investigated gravitational

lensing in different NUT metrics, to the best of my knowledge in the charged NUT–de Sitter metrics an exact analytic lens map has not been constructed so far. Therefore, the main aim of this paper is to use exact analytical methods to investigate gravitational lensing for arbitrary light rays in the charged NUT–de Sitter metrics. Geodesic motion in the NUT metric was first investigated by Zimmerman and Shahir [25]. After a thorough potential analysis Zimmerman and Shahir derived the time integral for radial timelike geodesics and investigated timelike circular and elliptic bound orbits. In addition they derived the deflection angle of light rays on spatial cones. The most thorough investigation of geodesic motion was carried out by Kagramanova *et al.* [14] using Weierstrass’ elliptic function and Weierstrass’ ζ and σ functions. However, for investigating gravitational lensing in the charged NUT–de Sitter metrics these functions are rather impractical because in the equations for the time coordinate derived in [14] during the integration procedure the branches of the logarithm have to be manually adjusted for each light ray individually. This problem can be circumvented by using the canonical forms of Legendre’s elliptic integrals and Jacobi’s elliptic functions. In general relativity using Legendre’s canonical forms of the elliptic integrals and Jacobi’s elliptic functions for solving the equations of motion has already a long tradition since the early 1920s. Forsyth [33], Morton [34], and Darwin [35] used Jacobi’s elliptic functions to solve and discuss lightlike and timelike geodesics in the Schwarzschild metric. More recently Yang and Wang [36] and Gralla and Lupsasca [37] extended these investigations to lightlike geodesics in the Kerr metric. In particular, the approach of Gralla and Lupsasca [37] can be easily transferred to lightlike geodesics in the charged NUT–de Sitter metrics. Therefore in the first part of this paper we will derive the solutions to the equations of motion in terms of Legendre’s elliptic integrals and Jacobi’s elliptic functions following the approach of Gralla and Lupsasca [37]. In the second part of the paper we will investigate gravitational lensing in the charged NUT–de Sitter metrics. We will construct an exact lens map following Frost and Perlick [38] using the tetrad approach of Grenzebach *et al.* [39]. We will use the tetrad approach to calculate the shadow of the black hole, set up a lens equation, and discuss the redshift and the travel time.

The remainder of this paper is structured as follows. In Sec. II we will summarize the main properties of the charged NUT–de Sitter metrics. In Sec. III we will discuss and solve the equations of motion. In Sec. IV we will set up the lens map and discuss lensing features in the charged NUT–de Sitter metrics, namely, the angular radius of the shadow, the lens equation, the redshift, and the travel time. We will also comment on how the observed lensing features can be used to measure the gravitomagnetic charge. In Sec. V we will summarize our results and conclusions. Throughout the paper we will use geometric units such that $c = G = 1$. The metric signature is $(-, +, +, +)$.

II. THE CHARGED NUT–de SITTER SPACETIME

The charged NUT–de Sitter metric belongs to the Plebański-Demiański family of electrovacuum spacetimes of Petrov type D [1] and is an exact solution of Einstein’s electrovacuum-field equations with cosmological constant. In Boyer-Lindquist-like coordinates its line element reads [8]

$$g_{\mu\nu}dx^\mu dx^\nu = -\frac{Q(r)}{\rho(r)}(dt + 2n(\cos\vartheta + C)d\varphi)^2 + \frac{\rho(r)}{Q(r)}dr^2 + \rho(r)(d\vartheta^2 + \sin^2\vartheta d\varphi^2), \quad (1)$$

where

$$Q(r) = -\frac{\Lambda}{3}r^4 + r^2(1 - 2\Lambda n^2) - 2mr + e^2 - n^2(1 - \Lambda n^2), \quad (2)$$

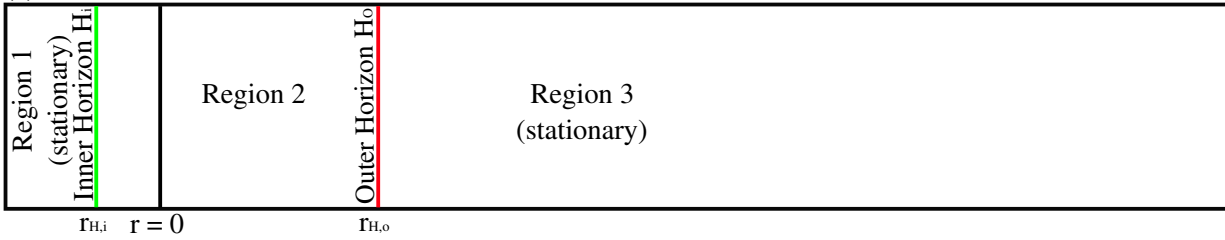
and

$$\rho(r) = r^2 + n^2. \quad (3)$$

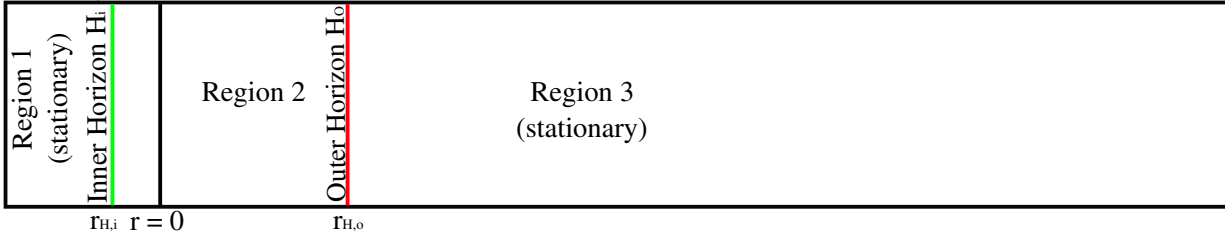
The metric is axisymmetric and stationary and for $\Lambda = 0$ asymptotically flat (note that here asymptotically flat means that the Riemann tensor vanishes but the spacetime is not asymptotically Minkowskian [5]). It contains five parameters: the mass parameter m , the cosmological constant Λ , the electric charge e , the gravitomagnetic charge n and the so-called Manko-Ruiz parameter C (for more information regarding the Manko-Ruiz parameter see [2]). When we set $n = 0$ the metric reduces to the Reissner-Nordström–de Sitter family of spacetimes which includes the Schwarzschild metric ($\Lambda = 0$ and $e = 0$), the Schwarzschild–de Sitter metric ($e = 0$) and the Reissner-Nordström metric ($\Lambda = 0$). For $e = 0$ and $\Lambda = 0$ the metric reduces to the standard NUT metric. For $e = 0$ it reduces to the NUT–de Sitter metric and for $\Lambda = 0$ it reduces to the charged NUT metric.

In this article we choose ϑ and φ such that they represent coordinates on the two-sphere S^2 and cover the range $\vartheta \in [0, \pi]$ and $\varphi \in [0, 2\pi)$. Although the spacetime is axisymmetric it retains some degree of “spherical symmetry.” As discussed in Newman *et al.* [4] for $C = -1$ and in Halla and Perlick [27] for arbitrary C the spacetime admits four linearly independent Killing vector fields. Three of these Killing vector fields generate isometries isomorphic to the rotation group $SO(3, \mathbb{R})$ and thus the metric is rotationally symmetric with respect to any radial direction (for more details see Halla and Perlick [27]). The Manko-Ruiz parameter C can be removed from Eq. (1) using the coordinate transformation $\tilde{t} = t + 2nC\varphi$. Note that this transformation is not valid globally because the φ coordinate is periodic and the time coordinate t is not.

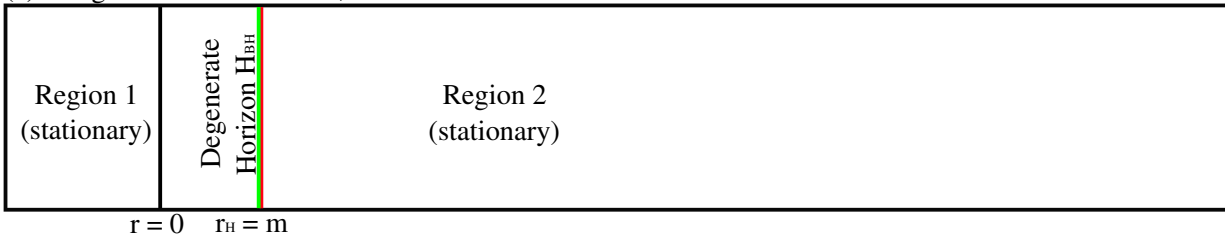
(a) NUT metric: $0 < n$



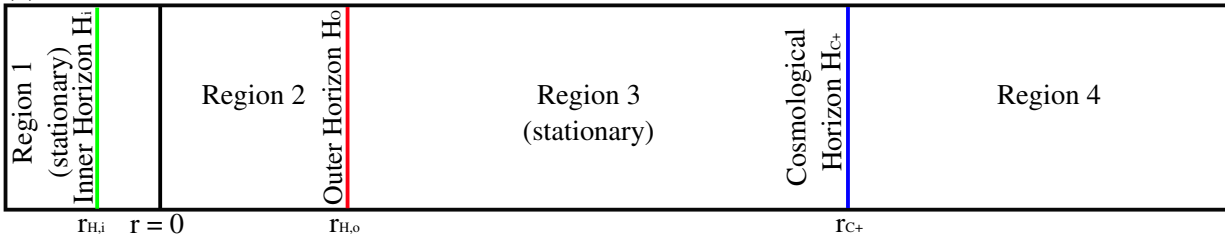
(b) charged NUT metric: $0 < n, 0 < e < e_c$



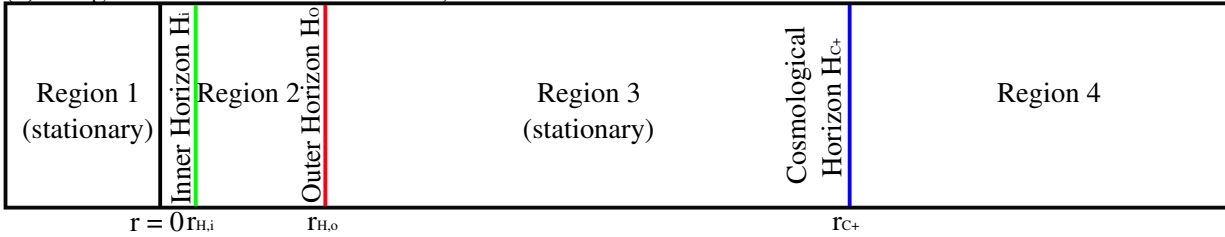
(c) charged NUT metric: $0 < n, e = e_c$



(d) NUT-de Sitter metric: $0 < n$



(e) charged NUT-de Sitter metric: $0 < n, 0 < e < e_c$



(f) charged NUT-de Sitter metric: $0 < n, e = e_c$

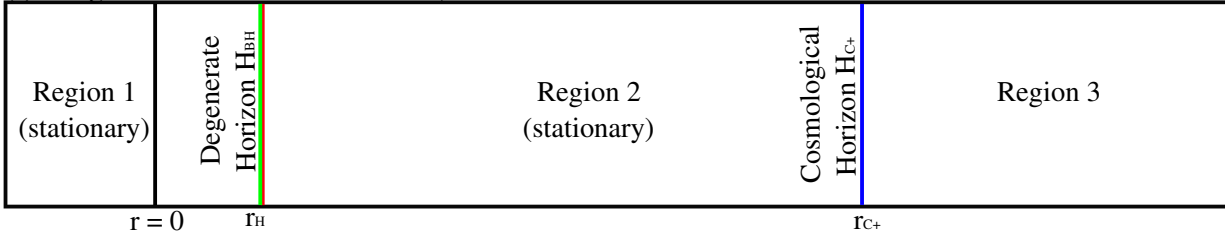


FIG. 1. Positions of the coordinate singularities in (a) the NUT metric, the charged NUT metric with (b) $0 < e < e_c = \sqrt{m^2 + n^2}$, and (c) $e = e_c = \sqrt{m^2 + n^2}$, (d) the NUT-de Sitter metric and the charged NUT-de Sitter metric with (e) $0 < e < e_c$ and (f) $e = e_c$. Note that the angular coordinates are suppressed and the cosmological horizon H_{C-} at r_{C-} , the region $r < r_{C-}$ and other singularities are not shown.

Therefore, charged NUT–de Sitter spacetimes with arbitrary C are locally isometric [31].

From the theoretical perspective the five parameters m , Λ , e , n , and C can take any arbitrary real value. Luckily the symmetries of the spacetime and observational experience allow us to reduce their range for our investigation of gravitational lensing. First, astronomical observations show that all objects in nature have a positive mass and thus we choose $m > 0$. Second, cosmological observations indicate that we live in an expanding Universe with positive cosmological constant allowing us to choose $0 \leq \Lambda < \Lambda_C$. Third, in Eq. (2) the electric charge e only enters as square and since we only deal with light rays we can choose $0 \leq e \leq e_C$ without loss of generality. Fourth and last, the gravitomagnetic charge n can be restricted considering the symmetries of the spacetime. When we set $n \rightarrow -n$, $C \rightarrow -C$ and perform the coordinate transformation $\vartheta \rightarrow \pi - \vartheta$ the line element remains invariant. Consequently we can limit the gravitomagnetic charge to $0 \leq n < n_C$ while the Manko-Ruiz parameter C can take any real number. Here, the three constants Λ_C , e_C , and n_C are limiting values that are determined by the nature of the desired spacetime. We will come back to these parameters when we discuss the singularities of the spacetime below. The charged NUT–de Sitter metric offers several mathematical peculiarities that may not be familiar to every reader. Thus in the following we will provide a short summary of its physical properties before we move on to discuss and solve the equations of motion.

The charged NUT–de Sitter metric admits several singularities. The line element Eq. (1) maintains its structure independent of how we choose Λ and e . Therefore, we will restrict our discussion to the NUT metric whenever possible. We start by discussing the singularities of the metric associated with the roots of $Q(r) = 0$. In the charged NUT–de Sitter metric the equation $Q(r) = 0$ can lead to up to four singularities. In this paper we want the metric to represent black hole spacetimes and thus we have to choose Λ_C , e_C and n_C such that all roots of the equation $Q(r) = 0$ are real. In this case all roots are coordinate singularities that can be removed using appropriate coordinate transformations. Figure 1 shows the horizon structures of the NUT metric [panel (a)], of the charged NUT metric [panels (b) and (c)], of the NUT–de Sitter metric [panel (d)] and of the charged NUT–de Sitter metric [panels (e) and (f)]. In the NUT metric Eq. (2) reduces to $Q(r) = r^2 - 2mr - n^2$. We can immediately read that it has two roots at

$$r_{\pm} = m \pm \sqrt{m^2 + n^2}. \quad (4)$$

For consistency with Fig. 1 from now on we will label them $r_- = r_{H,i}$ and $r_+ = r_{H,o}$. For $r < r_{H,i}$ and $r_{H,o} < r$ the vector field $K_t = \partial_t$ is timelike and the vector field $K_r = \partial_r$ is spacelike. In these two domains the spacetime is

stationary (except for a narrow region close to the Misner string as we will discuss below). The domain $r_{H,o} < r$ is usually referred to as domain of outer communication and will be of importance in Secs. III and IV. Between the horizons ∂_t is spacelike and ∂_r is timelike. In this domain the spacetime is nonstationary. When we add the electric charge e the horizon $r_{H,i}$ shifts to larger r and the horizon $r_{H,o}$ shifts to smaller r . When $e = e_C$ both horizons coincide at $r_H = m$. Adding the cosmological constant Λ gives rise to two additional, cosmological horizons r_{C-} and r_{C+} . Both cosmological horizons limit the stationary domains found in the NUT metric to $r_{C-} < r < r_{H,i}$ and $r_{H,o} < r < r_{C+}$. The two domains $r < r_{C-}$ and $r_{C+} < r$ are nonstationary. The function $\rho(r)$ is always positive. Consequently the charged NUT–de Sitter metric does not possess a curvature singularity at $r = 0$. This has an important implication for the whole spacetime. Lightlike and timelike geodesics are not blocked at $r = 0$ and thus the r coordinate covers the whole real axis ($r \in [-\infty, \infty]$).

In addition to the horizons the NUT metric has one or two conical singularities on the axes. The exact number depends on the Manko-Ruiz parameter C . For $C = 1$ the singularity is located on the axis $\vartheta = 0$. For $C = -1$ the spacetime has a singularity on the axis $\vartheta = \pi$. For all other choices of C the spacetime has singularities on both axes. For a more detailed discussion of the conical singularities see Jefremov and Perlick [40] and Halla and Perlick [27]. The allowed range of the time coordinate t depends on how the NUT metric is interpreted. As discussed before depending on the choice of the Manko-Ruiz parameter C the NUT metric has conical singularities (Misner strings) on one or both axes [2]. As discussed by Bonnor [6] the Misner strings can be interpreted as semi-infinite massless line sources of angular momentum and give rise to the gravitomagnetic charge. Following the approach of Misner [5] we can remove them by introducing a periodic time coordinate. But, this comes at a high price. In Misner's interpretation the periodic time coordinate leads to closed timelike curves in the whole spacetime. Closed timelike curves violate causality and are thus physically not desirable. Therefore in this paper we choose to retain the Misner strings and have $t \in \mathbb{R}$. In this case the spacetime also contains closed timelike curves whenever $g_{\varphi\varphi} \leq 0$ [6]; however, these are confined to very narrow regions close to the Misner strings.

III. EQUATIONS OF MOTION

For lightlike geodesics the charged NUT–de Sitter metric admits four constants of motion. These are the Lagrangian $\mathcal{L} = 0$, the energy of the light ray E , the angular momentum about the z axis L_z and the Carter constant K . The equations of motion are fully separable and read

$$\frac{dt}{d\lambda} = \frac{\rho(r)^2}{Q(r)} E - 2n(\cos \vartheta + C) \frac{L_z + 2n(\cos \vartheta + C)E}{\sin^2 \vartheta}, \quad (5)$$

$$\left(\frac{dr}{d\lambda}\right)^2 = \rho(r)^2 E^2 - Q(r)K, \quad (6)$$

$$\left(\frac{d\vartheta}{d\lambda}\right)^2 = K - \frac{(L_z + 2n(\cos\vartheta + C)E)^2}{\sin^2\vartheta}, \quad (7)$$

$$\frac{d\varphi}{d\lambda} = \frac{L_z + 2n(\cos\vartheta + C)E}{\sin^2\vartheta}. \quad (8)$$

The parameter λ is the Mino parameter [41]. It is defined up to an affine transformation and is related to the affine parameter s by

$$\frac{d\lambda}{ds} = \frac{1}{\rho(r)}. \quad (9)$$

Equations (7) and (8) are independent of Λ and e and as a consequence the conclusion of Clément *et al.* [15] that the φ coordinate is continuous for lightlike geodesics crossing the Misner strings is valid for all charged NUT–de Sitter metrics. The charged NUT–de Sitter metric does not possess an ergoregion and thus we are free to choose the sign of E ; however, to maintain comparability to Frost and Perlick [38,42] we will choose $E > 0$. This implies that for future-directed lightlike geodesics the Mino parameter λ is increasing and for past-directed lightlike geodesics the Mino parameter is decreasing. In the following we will first briefly discuss the equations of motion. We will derive the radius coordinate of the photon sphere and the angles of the

photon cones. We already have to note here that the latter will only be valid for individual light rays. We will discuss the turning points and solve the equations of motion for arbitrary initial conditions $(x_i^\mu) = (x^\mu(\lambda_i)) = (t_i, r_i, \vartheta_i, \varphi_i)$ following the procedures described in Gralla and Lupsasca [37] and Frost and Perlick [38,42]. In Sec. IV we will then use the obtained solutions to discuss gravitational lensing in the charged NUT–de Sitter metrics. For this purpose we only need the solutions to the equations of motion in the domain of outer communication. Therefore we will limit our discussion to lightlike geodesics with $r_{H,o} < r (< r_{C+})$.

A. The r motion

1. Potential and photon sphere

We begin with discussing the r motion. Following [38] we first rewrite Eq. (6) in terms of the potential $V_r(r)$:

$$\frac{1}{\rho(r)^2 K} \left(\frac{dr}{d\lambda}\right)^2 + V_r(r) = \frac{E^2}{K}, \quad (10)$$

where

$$V_r(r) = \frac{Q(r)}{\rho(r)^2}. \quad (11)$$

Figure 2 shows the potentials for the NUT metric (top left), the charged NUT metric (top right), the NUT–de Sitter metric (bottom left) and the charged NUT–de Sitter metric (bottom right) between the outer black hole horizon $r_{H,o}$ and $r = 25m$

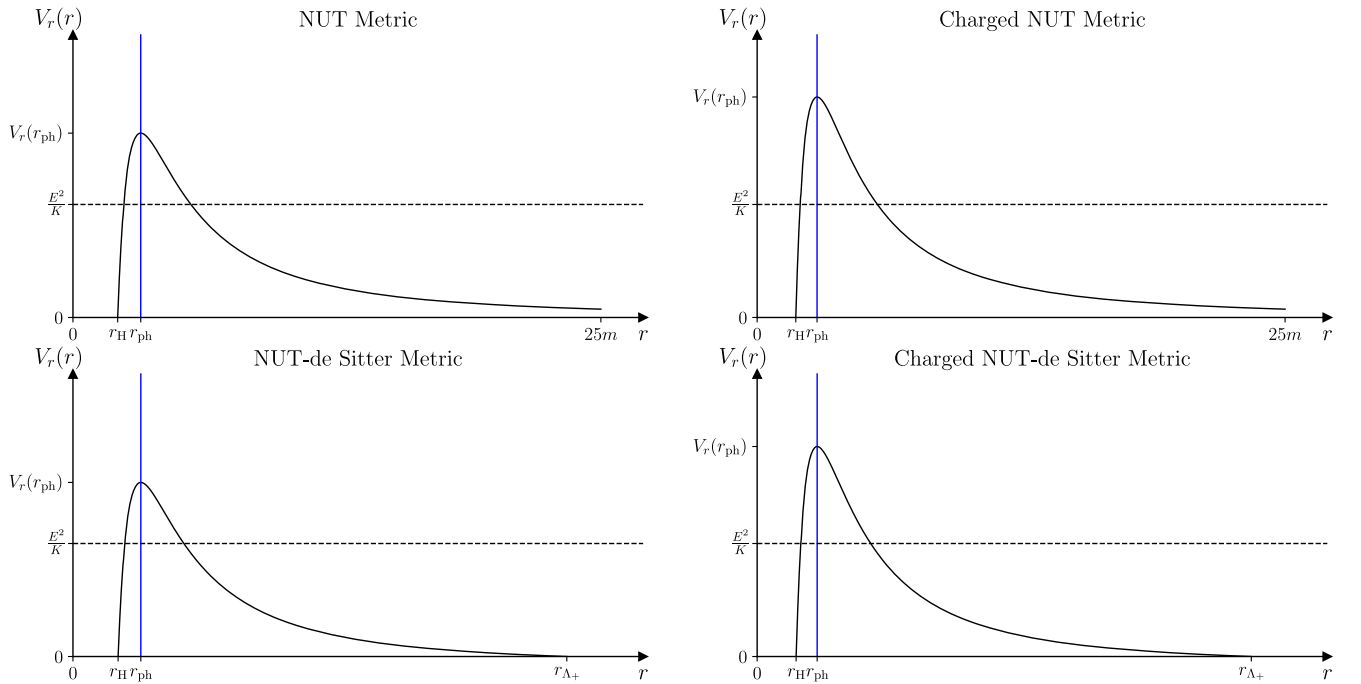


FIG. 2. Potential $V_r(r)$ of the r motion in the NUT metric (top left), the charged NUT metric (top right), the NUT–de Sitter metric (bottom left) and the charged NUT–de Sitter metric (bottom right) for $e = 3m/4$, $\Lambda = 1/(200m^2)$, and $n = m/2$. The axes have the same scale in all four plots. Note that due to spatial limitations we wrote r_H instead of $r_{H,o}$.

($\Lambda = 0$) or $r = r_{C+}$ ($0 < \Lambda < \Lambda_C$). We see that in the NUT metric (top left) the potential starts at $V_r(r_{H,o}) = 0$, has a maximum at $E^2/K = V_r(r_{ph})$ and then it falls off to $V_r(r) = 0$ for $r \rightarrow \infty$. When we turn on the electric charge e and the cosmological constant Λ the basic structure of the potential remains the same and we only observe small changes. When we turn on the electric charge e the maximum of $V_r(r)$ increases (top right). Turning on the cosmological constant on the other hand leads to a decrease of the maximum of $V_r(r)$ (bottom). In addition, for $0 < \Lambda < \Lambda_C$ we have $V_r(r_{C+}) = 0$ at the cosmological horizon r_{C+} .

At the maximum of $V_r(r)$ we have $dr/d\lambda = d^2r/d\lambda^2 = 0$. When we now combine these two constraints we obtain the determining relation for the radius coordinate of the photon sphere:

$$r^3 - \frac{3m}{1 - \frac{4}{3}\Lambda n^2} r^2 + \frac{2e^2 - 3n^2(1 - \frac{4}{3}\Lambda n^2)}{1 - \frac{4}{3}\Lambda n^2} r + \frac{mn^2}{1 - \frac{4}{3}\Lambda n^2} = 0. \quad (12)$$

In our Universe we can safely assume that the cosmological constant Λ and the gravitomagnetic charge n are very small. The consequence of this assumption is that the denominator of the coefficients is always positive and we can read from the structure of Eq. (12) that one solution is always real and negative. In addition we can either have a pair of complex conjugate roots or two real roots. In the following we agree to choose Λ , e and n such that we always have two real positive roots. We solve Eq. (12) using Cardano's method. We then label the three roots such that $r_{ph} > r_{ph+} > r_{ph-}$. The first root r_{ph} lies in the domain of outer communication. In terms of the mass parameter m and the gravitomagnetic charge n for the NUT metric it is explicitly given in Jefremov and Perlick [40] and for all NUT–de Sitter spacetimes it is also contained as special case in the results of Grenzebach *et al.* [31]. Because $V_r(r_{ph})$ has a maximum at r_{ph} this photon sphere is unstable. An infinitesimal radial perturbation of these orbits has the consequence that the light ray either falls into the black hole or escapes (across the cosmological horizon) to infinity. The second photon sphere r_{ph+} also lies at positive r and corresponds to a minimum of $V_r(r)$. Thus it is stable. The third photon sphere r_{ph-} lies in the region $r < 0$ and is again unstable. Figure 3 shows the radius coordinate of the photon sphere r_{ph} as function of the gravitomagnetic charge n for the NUT metric (black solid), the charged NUT metric (blue dashed), the NUT–de Sitter metric (green dotted) and the charged NUT–de Sitter metric (red dashed-dotted). For $e = 0$ and $n = 0$ (Schwarzschild–de Sitter limit) the photon sphere is located at the radius coordinate $r_{ph,S} = 3m$. For $e > 0$ and $n = 0$ (Reissner-Nordström–de Sitter limit) the photon sphere is located at the radius coordinate

$$r_{ph,RN} = \frac{3m + \sqrt{9m^2 - 8e^2}}{2}. \quad (13)$$

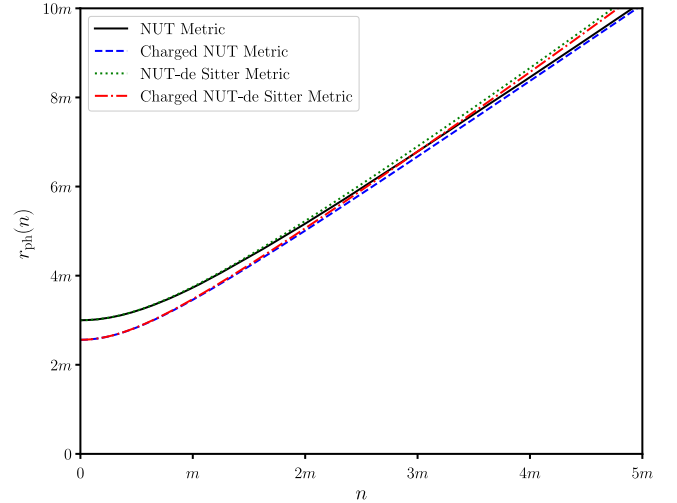


FIG. 3. Radius coordinate of the photon sphere $r_{ph}(n)$ as function of the gravitomagnetic charge n for the NUT metric (black solid), the charged NUT metric (blue dashed), the NUT–de Sitter metric (green dotted) and the charged NUT–de Sitter metric (red dashed-dotted). The electric charge and the cosmological constant are $e = 3m/4$ and $\Lambda = 1/(200m^2)$, respectively.

When we now turn on the gravitomagnetic charge n the photon sphere expands with increasing n . While this observation applies to all four spacetimes there are distinct differences when we turn on the electric charge e and the cosmological constant Λ . When we turn on the electric charge e (but still keep $\Lambda = 0$) for $n = 0$ the photon sphere is located at $r_{ph,RN} < r_{ph,S}$. With increasing gravitomagnetic charge the photon sphere expands and approaches the radius coordinate r_{ph} of the photon sphere in the NUT metric. When we turn on the cosmological constant we observe something similar. For $n = 0$ the photon spheres are located at $r_{ph,RN} < r_{ph,S}$. When we turn on the gravitomagnetic charge n both photon spheres expand and the radius coordinate r_{ph} of the photon sphere in the charged NUT–de Sitter metric approaches the radius coordinate r_{ph} of the photon sphere r_{ph} in the NUT–de Sitter metric. However, compared to the NUT metric and the charged NUT metric the photon spheres expand more rapidly with increasing gravitomagnetic charge n .

2. Types of motion

The potentials in Fig. 2 allow us to distinguish between the six following different types of motion in the domain of outer communication:

- (1) $E^2/K > V_r(r_{ph-})$ and $K = 0$: These geodesics do not have turning points in the domain of outer communication. We have one pair of complex conjugate purely imaginary double roots and label them such that $r_1 = r_3 = \bar{r}_2 = \bar{r}_4 = in$. These geodesics are the principal null geodesics of the charged NUT–de Sitter metrics.

- (2) $E^2/K > V_r(r_{\text{ph}-})$ and $K > 0$: These geodesics do not have turning points in the domain of outer communication. We have two pairs of complex conjugate roots. We label them such that $r_1 = \bar{r}_2 = R_1 + iR_2$ and $r_3 = \bar{r}_4 = R_3 + iR_4$. We always choose $R_1 < R_3$ and $R_2, R_4 > 0$.
- (3) $E^2/K = V_r(r_{\text{ph}-})$: These geodesics do not have turning points in the domain of outer communication. Two roots are real and equal. The other two roots are complex conjugate. We label the roots such that $r_1 = r_2 = r_{\text{ph}-}$ and $r_3 = \bar{r}_4 = R_3 + iR_4$. We always choose $R_4 > 0$.
- (4) $V_r(r_{\text{ph}-}) > E^2/K > V_r(r_{\text{ph}})$: These geodesics do not have turning points in the domain of outer communication. Two roots are real and two roots are complex conjugate. We label the roots such that $r_1 > r_2$ and $r_3 = \bar{r}_4 = R_3 + iR_4$. We always choose $R_4 > 0$.
- (5) $E^2/K = V_r(r_{\text{ph}})$: These geodesics do not have turning points in the domain of outer communication but four real roots. We label the roots such that $r_1 = r_2 = r_{\text{ph}} > r_3 > r_4$. These geodesics asymptotically come from or go to the photon sphere.
- (6) $V_r(r_{\text{ph}}) > E^2/K$: These geodesics have turning points in the domain of outer communication. All four roots are real. We label the roots such that $r_1 > r_2 > r_3 > r_4$. For $r_{\text{H},0} < r < r_{\text{ph}}$ these geodesics have a maximum at $r_{\text{max}} = r_2$. For $r_{\text{ph}} < r (< r_{\text{C}+})$ these geodesics have a minimum at $r_{\text{min}} = r_1$.

3. Calculating $r(\lambda)$

Case 1: We have $E^2/K > V_r(r_{\text{ph}-})$ and $K = 0$. We will see in Sec. III B that these geodesics are the principal null geodesics of the charged NUT–de Sitter metrics. In Eq. (6) we first set $K = 0$ and get

$$\left(\frac{dr}{d\lambda}\right)^2 = \rho(r)^2 E^2. \quad (14)$$

Equation (14) can be solved in terms of elementary functions. We first separate variables and integrate. Then we solve for r . With $i_{r_i} = \text{sgn}(dr/d\lambda|_{r=r_i})$ the solution reads

$$r(\lambda) = n \tan \left(\arctan \left(\frac{r_i}{n} \right) + i_{r_i} n E (\lambda - \lambda_i) \right). \quad (15)$$

Case 2: Lightlike geodesics with $E^2/K > V_r(r_{\text{ph}-})$ and $K > 0$ have no turning points in the domain of outer communication. Here we first define two new constants of motion [37,43]:

$$S = \sqrt{(R_2 - R_4)^2 + (R_1 - R_3)^2}, \quad (16)$$

and

$$\bar{S} = \sqrt{(R_2 + R_4)^2 + (R_1 - R_3)^2}, \quad (17)$$

and substitute

$$r = R_1 - R_2 \frac{g_0 - \tan \chi}{1 + g_0 \tan \chi}, \quad (18)$$

where

$$g_0 = \sqrt{\frac{4R_2^2 - (S - \bar{S})^2}{(S + \bar{S})^2 - 4R_2^2}} \quad (19)$$

to put Eq. (6) in the Legendre form Eq. (B9). Now we follow the steps described in Appendix B and obtain the solution $r(\lambda)$ in terms of Jacobi's elliptic sc function

$$r(\lambda) = R_1 - R_2 \frac{g_0 - \text{sc} \left(i_{r_i} \sqrt{E^2 + \frac{\Lambda}{3} K} \frac{S + \bar{S}}{2} (\lambda - \lambda_i) + \lambda_{r_i, k_1}, k_1 \right)}{1 + g_0 \text{sc} \left(i_{r_i} \sqrt{E^2 + \frac{\Lambda}{3} K} \frac{S + \bar{S}}{2} (\lambda - \lambda_i) + \lambda_{r_i, k_1}, k_1 \right)}, \quad (20)$$

where λ_{r_i, k_1} , the initial condition χ_i and the square of the elliptic modulus k_1 are given by

$$\lambda_{r_i, k_1} = F_L(\chi_i, k_1), \quad (21)$$

$$\chi_i = \arctan \left(\frac{r_i - R_1}{R_2} \right) + \arctan(g_0), \quad (22)$$

and

$$k_1 = \frac{4S\bar{S}}{(S + \bar{S})^2}. \quad (23)$$

Case 3: Lightlike geodesics with $E^2/K = V_r(r_{\text{ph}-})$ have two equal roots at $r_1 = r_2 = r_{\text{ph}-}$. We first express the right-hand side of Eq. (6) in terms of the roots. Then we separate variables and integrate from $r(\lambda_i) = r_i$ to $r(\lambda)$ and obtain

$$\lambda - \lambda_i = \frac{i_{r_i}}{\sqrt{E^2 + \frac{\Lambda}{3} K}} \int_{r_i}^{r(\lambda)} \frac{dr'}{(r' - r_1) \sqrt{(R_3 - r')^2 + R_4^2}}. \quad (24)$$

The integral on the right-hand side of Eq. (24) has the form of Eq. (A3). Now we follow the steps described in Appendix A 1 a and integrate. Then we insert Eq. (A3), solve for r and obtain

$$r(\lambda) = r_1 + \frac{(R_3 - r_1)^2 + R_4^2}{R_3 - r_1 + R_4 \sinh \left(\operatorname{arsinh} \left(\frac{r_1 - R_3}{R_4} + \frac{(R_3 - r_1)^2 + R_4^2}{R_4(r_i - r_1)} \right) - i_{r_i} \sqrt{(E^2 + \frac{\Lambda}{3}K)((R_3 - r_1)^2 + R_4^2)(\lambda - \lambda_i)} \right)}. \quad (25)$$

Case 4: Lightlike geodesics with $V_r(r_{\text{ph}-}) > E^2/K > V_r(r_{\text{ph}})$ have no turning points in the domain of outer communication. Two of the roots are real. Using the two real roots r_1 and r_2 and the real and imaginary parts R_3 and R_4 of the complex conjugate roots r_3 and r_4 we first define two new constants of motion R and \bar{R} :

$$R = \sqrt{(R_3 - r_1)^2 + R_4^2}, \quad (26)$$

$$\bar{R} = \sqrt{(R_3 - r_2)^2 + R_4^2}. \quad (27)$$

Then we use the transformation [37,44]

$$r = \frac{r_1 \bar{R} - r_2 R + (r_1 \bar{R} + r_2 R) \cos \chi}{\bar{R} - R + (\bar{R} + R) \cos \chi} \quad (28)$$

to put Eq. (6) into the Legendre form Eq. (B9). Then we follow the steps described in Appendix B to obtain $r(\lambda)$ in terms of Jacobi's elliptic cn function:

$$r(\lambda) = \frac{r_1 \bar{R} - r_2 R + (r_1 \bar{R} + r_2 R) \operatorname{cn}(i_{r_i} \sqrt{(E^2 + \frac{\Lambda}{3}K)R\bar{R}(\lambda - \lambda_i)} + \lambda_{r_i, k_2}, k_2)}{\bar{R} - R + (\bar{R} + R) \operatorname{cn}(i_{r_i} \sqrt{(E^2 + \frac{\Lambda}{3}K)R\bar{R}(\lambda - \lambda_i)} + \lambda_{r_i, k_2}, k_2)}, \quad (29)$$

where λ_{r_i, k_2} , the initial condition χ_i and the square of the elliptic modulus k_2 are given by

$$\lambda_{r_i, k_2} = F_L(\chi_i, k_2), \quad (30)$$

$$\chi_i = \arccos \left(\frac{(r_i - r_2)R - (r_i - r_1)\bar{R}}{(r_i - r_2)R + (r_i - r_1)\bar{R}} \right), \quad (31)$$

and

$$k_2 = \frac{(R + \bar{R})^2 - (r_1 - r_2)^2}{4R\bar{R}}. \quad (32)$$

Case 5: Lightlike geodesics with $E^2/K = V_r(r_{\text{ph}})$ have two equal roots at $r_1 = r_2 = r_{\text{ph}} > r_3 > r_4$. These are either lightlike geodesics trapped on the photon sphere $r = r_{\text{ph}}$ or lightlike geodesics asymptotically coming from or going to the photon sphere. In the former case the solution to Eq. (6) is $r(\lambda) = r_{\text{ph}}$. In the latter case we first rewrite the right-hand side of Eq. (6) in terms of the roots

$$\left(\frac{dr}{d\lambda} \right)^2 = \left(E^2 + \frac{\Lambda}{3}K \right) (r - r_{\text{ph}})^2 (r - r_3) (r - r_4). \quad (33)$$

Now we substitute

$$r = r_3 + \frac{3a_{3,r}}{12y - a_{2,r}}, \quad (34)$$

where

$$a_{2,r} = 6 \left(E^2 + \frac{\Lambda}{3}K \right) r_3^2 + 2n^2 E^2 - (1 - 2\Lambda n^2)K, \quad (35)$$

$$a_{3,r} = 4 \left(E^2 + \frac{\Lambda}{3}K \right) r_3^3 + 2(2n^2 E^2 - (1 - 2\Lambda n^2)K)r_3 + 2mK, \quad (36)$$

and obtain

$$\left(\frac{dy}{d\lambda} \right)^2 = 4(y - y_{\text{ph}})^2 (y - y_1). \quad (37)$$

y_{ph} and y_1 are related to the radius coordinate of the photon sphere r_{ph} and the root r_4 by Eq. (34), respectively. It is easy to show that $y_1 < y_{\text{ph}}$ and $y_1 < y$. Now we have to distinguish between lightlike geodesics between outer black hole horizon $r_{\text{H},0}$ and photon sphere r_{ph} and lightlike geodesics between photon sphere r_{ph} and infinity ($\Lambda = 0$) or cosmological horizon $r_{\text{C}+}$ ($0 < \Lambda < \Lambda_{\text{C}}$). In the former case we have $y_{\text{ph}} < y$ and in the latter case we have $y < y_{\text{ph}}$. Now we separate variables and integrate from $y(\lambda_i) = y_i$ to $y(\lambda)$ and obtain

$$\lambda - \lambda_i = -\frac{i_{r_i}}{2} \int_{y_i}^{y(\lambda)} \frac{dy'}{\sqrt{(y' - y_{\text{ph}})^2 (y' - y_1)}}. \quad (38)$$

For $r_{\text{H},0} < r < r_{\text{ph}}$ we rewrite the right-hand side of Eq. (38) in terms of the integral I_6 given by Eq. (A6) in Appendix A 1 b. Now we follow the steps described in Appendix A 1 b and obtain the right-hand side of Eq. (A6). After inserting I_6 in Eq. (38) we solve for r and obtain

$$r(\lambda) = r_3 - \frac{(r_{\text{ph}} - r_3)(r_3 - r_4)}{r_{\text{ph}} - r_3 - (r_{\text{ph}} - r_4) \coth^2 \left(\operatorname{arcoth} \left(\sqrt{\frac{(r_i - r_4)(r_{\text{ph}} - r_3)}{(r_i - r_3)(r_{\text{ph}} - r_4)}} \right) + i_{r_i} \sqrt{a_r} (\lambda - \lambda_i) \right)}, \quad (39)$$

where

$$a_r = \frac{(2(E^2 + \frac{\Lambda}{3}K)r_3^3 + (2n^2E^2 - (1 - 2\Lambda n^2)K)r_3 + mK)(r_{\text{ph}} - r_4)}{2(r_{\text{ph}} - r_3)(r_3 - r_4)}. \quad (40)$$

Analogously for $r_{\text{ph}} < r (< r_{\text{C}+})$ we rewrite the right-hand side of Eq. (38) in terms of the integral I_8 given by Eq. (A8) in Appendix A 1 b. Again we integrate following the steps described in Appendix A 1 b and obtain the right-hand side of Eq. (A8). After inserting I_8 in Eq. (38) we solve for r and obtain

$$r(\lambda) = r_3 - \frac{(r_{\text{ph}} - r_3)(r_3 - r_4)}{r_{\text{ph}} - r_3 - (r_{\text{ph}} - r_4) \tanh^2 \left(\operatorname{artanh} \left(\sqrt{\frac{(r_i - r_4)(r_{\text{ph}} - r_3)}{(r_i - r_3)(r_{\text{ph}} - r_4)}} \right) - i_{r_i} \sqrt{a_r} (\lambda - \lambda_i) \right)}. \quad (41)$$

Case 6: Lightlike geodesics with $V_r(r_{\text{ph}}) > E^2/K$ have turning points in the domain of outer communication. We have to distinguish between lightlike geodesics between outer black hole horizon $r_{\text{H},0}$ and photon sphere r_{ph} and lightlike geodesics between photon sphere r_{ph} and infinity ($\Lambda = 0$) or the cosmological horizon $r_{\text{C}+}$ ($0 < \Lambda < \Lambda_{\text{C}}$). We start with solving Eq. (6) for lightlike geodesics in the domain $r_{\text{H},0} < r < r_{\text{ph}}$. Here we first substitute [37,44]

$$r = r_1 - \frac{(r_1 - r_2)(r_1 - r_3)}{r_1 - r_3 - (r_2 - r_3) \sin^2 \chi} \quad (42)$$

to put Eq. (6) into the Legendre form Eq. (B9). Then we follow the steps described in Appendix B to obtain $r(\lambda)$ in terms of Jacobi's elliptic sn function:

$$r(\lambda) = r_1 - \frac{(r_1 - r_2)(r_1 - r_3)}{r_1 - r_3 - (r_2 - r_3) \operatorname{sn}^2 \left(\frac{i_{r_i}}{2} \sqrt{(E^2 + \frac{\Lambda}{3}K)(r_1 - r_3)(r_2 - r_4)} (\lambda_i - \lambda) + \lambda_{r_i, k_3}, k_3 \right)}, \quad (43)$$

where λ_{r_i, k_3} , the initial condition χ_i and the square of the elliptic modulus k_3 are given by

$$\lambda_{r_i, k_3} = F_L(\chi_i, k_3), \quad (44)$$

$$\chi_i = \arcsin \left(\sqrt{\frac{(r_2 - r_i)(r_1 - r_3)}{(r_1 - r_i)(r_2 - r_3)}} \right), \quad (45)$$

and

$$k_3 = \frac{(r_2 - r_3)(r_1 - r_4)}{(r_1 - r_3)(r_2 - r_4)}. \quad (46)$$

Analogously for $r_{\text{ph}} < r (< r_{\text{C}+})$ we first substitute [37,44]

$$r = r_2 + \frac{(r_1 - r_2)(r_2 - r_4)}{r_2 - r_4 - (r_1 - r_4) \sin^2 \chi} \quad (47)$$

to put Eq. (6) into the Legendre form Eq. (B9). Then we again follow the steps described in Appendix B and obtain $r(\lambda)$ in terms of Jacobi's elliptic sn function:

$$r(\lambda) = r_2 + \frac{(r_1 - r_2)(r_2 - r_4)}{r_2 - r_4 - (r_1 - r_4)\text{sn}^2\left(\frac{i_{r_i}}{2}\sqrt{(E^2 + \frac{\Lambda}{3}K)(r_1 - r_3)(r_2 - r_4)(\lambda - \lambda_i) + \lambda_{r_i, k_3}, k_3}\right)}. \quad (48)$$

Here λ_{r_i, k_3} and k_3 are given by Eq. (44) and Eq. (46), respectively, and the initial condition χ_i reads

$$\chi_i = \arcsin\left(\sqrt{\frac{(r_i - r_1)(r_2 - r_4)}{(r_i - r_2)(r_1 - r_4)}}\right). \quad (49)$$

B. The ϑ motion

For discussing the ϑ motion we first rewrite Eq. (7) in terms of $x = \cos \vartheta$:

$$\left(\frac{dx}{d\lambda}\right)^2 = (1 - x^2)K - (L_z + 2n(x + C)E)^2. \quad (50)$$

From the structure of Eq. (50) we can immediately read that for $K = 0$ the right-hand side has to vanish. This simultaneously implies that we have $d\varphi/d\lambda = 0$ and thus these are the principal null geodesics of the charged NUT–de Sitter metrics. Similarly it is very easy to show that for very specific combinations of the constants of motion the right-hand side of Eq. (50) vanishes. In both cases the lightlike geodesics lie on cones of constant ϑ that have to fulfill the constraints $dx/d\lambda = d^2x/d\lambda^2 = 0$. From the second

constraint we now immediately obtain the angle of the cones in terms of the constants of motion. It reads

$$\vartheta_{\text{ph}} = \arccos\left(-\frac{2nE(2nEC + L_z)}{4n^2E^2 + K}\right). \quad (51)$$

Under the premise that we have $K \neq 0$ we can use both constraints to rewrite the Carter constant K in terms of E and L_z :

$$K = (2nEC + L_z)^2 - 4n^2E^2. \quad (52)$$

In analogy to the charged C–de Sitter metrics discussed in Frost and Perlick [38] and Frost [42] we will call these cones *individual photon cones*. However, we have to emphasize that contrary to the charged C–de Sitter metrics in which all geodesics tangential to the photon cone remain on the photon cone, in the charged NUT–de Sitter metrics this is only the case for very specific lightlike geodesics. In both cases, the principal null geodesics and the geodesics on the photon cones, the solution to Eq. (7) is easy to obtain. It reads $\vartheta(\lambda) = \vartheta_i$. All other geodesics oscillate between the two turning points,

$$x_{\min} = \cos \vartheta_{\min} = \frac{\sqrt{K(K + 4n^2E^2 - (2nEC + L_z)^2)} - 2nE(2nEC + L_z)}{K + 4n^2E^2}, \quad (53)$$

$$x_{\max} = \cos \vartheta_{\max} = -\frac{\sqrt{K(K + 4n^2E^2 - (2nEC + L_z)^2)} + 2nE(2nEC + L_z)}{K + 4n^2E^2}. \quad (54)$$

As we can see $x_{\min} \neq -x_{\max}$ and thus the ϑ motion is not symmetric with respect to the plane $\vartheta = \pi/2$. For these geodesics we can rewrite Eq. (50) in terms of an elementary integral that can be easily calculated. After the integration we solve for ϑ and obtain as solution to Eq. (7)

$$\vartheta(\lambda) = \arccos\left(\frac{\sqrt{K(K + 4n^2E^2 - (2nEC + L_z)^2)}}{K + 4n^2E^2}\sin(a_\vartheta - i_{\vartheta_i}\sqrt{K + 4n^2E^2}(\lambda - \lambda_i)) - \frac{2nE(2nEC + L_z)}{K + 4n^2E^2}\right), \quad (55)$$

where

$$a_\vartheta = \arcsin\left(\frac{(K + 4n^2E^2)\cos \vartheta_i + 2nE(2nEC + L_z)}{\sqrt{K(K + 4n^2E^2 - (2nEC + L_z)^2)}}\right), \quad (56)$$

and $i_{\vartheta_i} = \text{sgn}(d\vartheta/d\lambda|_{\vartheta=\vartheta_i})$. Structurally this solution is the same as Eq. (32) in Kagramanova *et al.* [14] and it can be easily rewritten in the form of Eq. (3.12) in Clément *et al.* [15].

C. The φ motion

For properly discussing the φ motion in the charged NUT–de Sitter metrics we have to consider several peculiarities. As stated in Zimmerman and Shahir [25] and in Halla and Perlick [27], all lightlike geodesics are contained in cones. These cones can point in arbitrary directions and therefore lightlike geodesics can orbit any axis in space. This has the consequence that not all geodesics perform a full 2π orbit about the z axis. When the cones point away from the z axis and the axis is not enclosed by the cone the

φ motion reverses and the geodesic changes direction. In addition it has long been an open question if the Misner strings are transparent or opaque. When they are opaque all lightlike geodesics terminate at the Misner strings and cannot be continued. In this case the Misner strings cast a shadow. However, Clément *et al.* [15] demonstrated that for lightlike geodesics crossing the Misner strings the φ motion is continuous. This strongly advocates that it is transparent. Therefore, in this paper we will assume that the Misner strings are transparent and do not cast a shadow.

When we want to integrate Eq. (8) we have to distinguish the same three types of motion as in Sec. III B for ϑ . We start with the principal null geodesics. Principal null geodesics have $K = 0$ and the right-hand side of Eq. (8) vanishes. Therefore the solution to Eq. (8) simply reads $\varphi(\lambda) = \varphi_i$. In the second case we have $K = (2nEC + L_z)^2 - 4n^2E^2$. These are geodesics moving on *individual photon cones*. Here, the right-hand side of Eq. (8) is constant and after a simple integration the solution reads

$$\varphi(\lambda) = \varphi_i + \frac{(L_z + 2n(\cos \vartheta_{\text{ph}} + C)E)(\lambda - \lambda_i)}{\sin^2 \vartheta_{\text{ph}}}. \quad (57)$$

All other geodesics oscillate between the turning points ϑ_{min} and ϑ_{max} of the ϑ motion. Here, we proceed as follows. We first replace $x = \cos \vartheta$ on the right-hand side of Eq. (8):

$$\frac{d\varphi}{d\lambda} = \frac{L_z + 2n(x + C)E}{1 - x^2}. \quad (58)$$

Now we perform a partial fraction decomposition,

$$\frac{1}{1 - x^2} = \frac{1}{2} \left(\frac{1}{1 - x} + \frac{1}{1 + x} \right), \quad (59)$$

and rewrite Eq. (58) as

$$\frac{d\varphi}{d\lambda} = \frac{L_z + 2nE(1 + C)}{2(1 - x)} + \frac{L_z - 2nE(1 - C)}{2(1 + x)}. \quad (60)$$

Now we resubstitute $x = \cos \vartheta$ and insert Eq. (55) in Eq. (60). Then we integrate over λ . The solution to Eq. (8) now reads [see also Eq. (43) in Kagramanova *et al.* [14] and Eq. (3.16) in Clément *et al.* [15] for alternative formulations]

$$\begin{aligned} \varphi(\lambda) = & \varphi_i + i_{\vartheta_i} \left(\arctan \left(c_{\vartheta,1} \left(\tan \left(\frac{\tilde{\lambda}(\lambda_i)}{2} \right) - c_{\vartheta,2} \right) \right) - \arctan \left(c_{\vartheta,1} \left(\tan \left(\frac{\tilde{\lambda}(\lambda)}{2} \right) - c_{\vartheta,2} \right) \right) \right. \\ & \left. + \arctan \left(c_{\vartheta,3} \left(\tan \left(\frac{\tilde{\lambda}(\lambda)}{2} \right) + c_{\vartheta,4} \right) \right) - \arctan \left(c_{\vartheta,3} \left(\tan \left(\frac{\tilde{\lambda}(\lambda_i)}{2} \right) + c_{\vartheta,4} \right) \right) \right), \end{aligned} \quad (61)$$

where $c_{\vartheta,1}$, $c_{\vartheta,2}$, $c_{\vartheta,3}$, $c_{\vartheta,4}$ and $\tilde{\lambda}(\lambda)$ are given by

$$c_{\vartheta,1} = \frac{K + 4n^2E^2 + 2nE(2nEC + L_z)}{\sqrt{K + 4n^2E^2(2nE(1 + C) + L_z)}}, \quad c_{\vartheta,2} = \frac{\sqrt{K(K + 4n^2E^2 - (2nEC + L_z)^2)}}{K + 4n^2E^2 + 2nE(2nEC + L_z)}, \quad (62)$$

$$c_{\vartheta,3} = \frac{K + 4n^2E^2 - 2nE(2nEC + L_z)}{\sqrt{K + 4n^2E^2(2nE(1 - C) - L_z)}}, \quad c_{\vartheta,4} = \frac{\sqrt{K(K + 4n^2E^2 - (2nEC + L_z)^2)}}{K + 4n^2E^2 - 2nE(2nEC + L_z)}, \quad (63)$$

$$\tilde{\lambda}(\lambda) = \arcsin \left(\frac{(K + 4n^2E^2) \cos \vartheta_i + 2nE(2nEC + L_z)}{\sqrt{K(K + 4n^2E^2 - (2nEC + L_z)^2)}} \right) - i_{\vartheta_i} \sqrt{K + 4n^2E^2} (\lambda - \lambda_i). \quad (64)$$

Note that for the explicit calculation of $\varphi(\lambda)$ the multivaluedness of the arctan has to be appropriately considered.

D. The time coordinate t

Equation (5) has two terms that separately depend on r and ϑ . In the following we will demonstrate how to calculate both components. For this purpose we first integrate Eq. (5) over λ and rewrite it as follows:

$$t(\lambda) = t_i + t_r(\lambda) + t_{\vartheta}(\lambda), \quad (65)$$

where the r -dependent integral reads

$$t_r(\lambda) = \int_{\lambda_i}^{\lambda} \frac{\rho(r(\lambda'))^2 E d\lambda'}{Q(r(\lambda'))}, \quad (66)$$

and the ϑ -dependent integral reads

$$t_{\vartheta}(\lambda) = -2n \int_{\lambda_i}^{\lambda} (\cos \vartheta(\lambda') + C) \frac{(L_z + 2n(\cos \vartheta(\lambda') + C)E) d\lambda'}{1 - \cos^2 \vartheta(\lambda')}. \quad (67)$$

1. Calculating $t_\vartheta(\lambda)$

We start with evaluating the integral on the right-hand side of $t_\vartheta(\lambda)$ in Eq. (67). We have to distinguish the same three different types of motion as in Sec. III B for the ϑ motion. For $K = 0$ the right-hand side of Eq. (67) vanishes and we have $t_\vartheta(\lambda) = 0$. For lightlike geodesics on *individual photon cones* we have $K = (2nEC + L_z)^2 - 4n^2E^2$ and thus the right-hand side of Eq. (67) is constant. We integrate over λ and get

$$t_\vartheta(\lambda) = -2n(\cos\vartheta_{\text{ph}} + C) \frac{(L_z + 2n(\cos\vartheta_{\text{ph}} + C)E)(\lambda - \lambda_i)}{\sin^2\vartheta_{\text{ph}}}. \quad (68)$$

In all remaining cases the lightlike geodesics oscillate between the turning points ϑ_{min} and ϑ_{max} . Here we first substitute $x = \cos\vartheta$ and perform a partial fraction decomposition using Eq. (59). We restructure and integrate the constant term. Now $t_\vartheta(\lambda)$ reads

$$t_\vartheta(\lambda) = 4n^2E(\lambda - \lambda_i) + n \left((1 - C)(L_z - 2nE(1 - C)) \int_{\lambda_i}^{\lambda} \frac{d\lambda'}{1 + x(\lambda')} - (1 + C)(L_z + 2nE(1 + C)) \int_{\lambda_i}^{\lambda} \frac{d\lambda'}{1 - x(\lambda')} \right). \quad (69)$$

Now we insert $x(\lambda) = \cos\vartheta(\lambda)$ and calculate the remaining two integrals. After integration $t_\vartheta(\lambda)$ reads

$$t_\vartheta(\lambda) = 4n^2E(\lambda - \lambda_i) + i_{\vartheta_i} 2n \left((1 - C) \left(\arctan \left(c_{\vartheta,3} \left(\tan \left(\frac{\tilde{\lambda}(\lambda)}{2} \right) + c_{\vartheta,4} \right) \right) - \arctan \left(c_{\vartheta,3} \left(\tan \left(\frac{\tilde{\lambda}(\lambda_i)}{2} \right) + c_{\vartheta,4} \right) \right) \right) \right. \\ \left. + (1 + C) \left(\arctan \left(c_{\vartheta,1} \left(\tan \left(\frac{\tilde{\lambda}(\lambda)}{2} \right) - c_{\vartheta,2} \right) \right) - \arctan \left(c_{\vartheta,1} \left(\tan \left(\frac{\tilde{\lambda}(\lambda_i)}{2} \right) - c_{\vartheta,2} \right) \right) \right) \right), \quad (70)$$

where the coefficients $c_{\vartheta,1}$, $c_{\vartheta,2}$, $c_{\vartheta,3}$ and $c_{\vartheta,4}$ are given by Eqs. (62) and (63) and $\tilde{\lambda}(\lambda)$ is given by Eq. (64). Note that for the explicit calculation of $t_\vartheta(\lambda)$ the multivaluedness of the arctan has to be appropriately considered. In addition we note that structurally Eq. (70) is the same as Eq. (45) in Kagramanova *et al.* [14] and Eq. (4.23) in Clément *et al.* [15].

2. Calculating $t_r(\lambda)$

Now we turn to the r -dependent part of the time coordinate $t_r(\lambda)$. Here we have to distinguish the same six types of motion as for the r motion. We start by separating variables in Eq. (6). Then we rewrite Eq. (66) as integral over r . Now it reads

$$t_r(\lambda) = \int_{r_i \dots}^{\dots r(\lambda)} \frac{\rho(r')^2 E dr'}{Q(r') \sqrt{\rho(r')^2 E^2 - Q(r') K}}. \quad (71)$$

Here, the dots in the limits shall indicate that we have to split the integral at the turning points and the sign of the root in the denominator has to be chosen according to the direction of the r motion. In addition for explicitly integrating Eq. (71) for each type of motion we have to distinguish four different cases. These are $r_{\text{H},i} < r_{\text{H},o}$ for the NUT metric and the charged NUT metric, $r_{\text{H},i} = r_{\text{H},o} = r_{\text{H}}$ for the extremally charged NUT metric, $r_{\text{C}-} < r_{\text{H},i} < r_{\text{H},o} < r_{\text{C}+}$ for the NUT–de Sitter metric and the charged NUT–de Sitter metric and $r_{\text{C}-} < r_{\text{H},i} = r_{\text{H},o} = r_{\text{H}} < r_{\text{C}+}$ for the extremally charged NUT–de Sitter metric. Due to the sheer number of integrals we cannot explicitly demonstrate how to calculate each of them here. We only provide the exact

equations for the time coordinate in all four cases for the principal null geodesics. For all other types of motion we only briefly describe the steps of the integration procedure. We proceed in the same order as in Sec. III A.

Case 1: We start with the principal null geodesics with $E^2/K > V_r(r_{\text{ph}-})$ and $K = 0$. In this case Eq. (71) reduces to

$$t_r(\lambda) = i_{r_i} \int_{r_i}^{r(\lambda)} \frac{\rho(r') dr'}{Q(r')}. \quad (72)$$

Now we restructure $\rho(r')/Q(r')$ such that only terms with r' in the nominator or the denominator remain. Then we perform a partial fraction decomposition and integrate. The resulting expressions for $t_r(\lambda)$ are given in terms of simple elementary functions. In the case of the NUT metric and the charged NUT metric with $r_{\text{H},i} < r_{\text{H},o}$ $t_r(\lambda)$ reads

$$t_r(\lambda) = i_{r_i} \left(r(\lambda) - r_i + \frac{r_{\text{H},o}^2 + n^2}{r_{\text{H},o} - r_{\text{H},i}} \ln \left(\frac{r(\lambda) - r_{\text{H},o}}{r_i - r_{\text{H},o}} \right) \right. \\ \left. + \frac{r_{\text{H},i}^2 + n^2}{r_{\text{H},o} - r_{\text{H},i}} \ln \left(\frac{r_i - r_{\text{H},i}}{r(\lambda) - r_{\text{H},i}} \right) \right), \quad (73)$$

while for the extremally charged NUT metric with $r_{\text{H},i} = r_{\text{H},o} = r_{\text{H}}$ it reads

$$t_r(\lambda) = i_{r_i} \left(r(\lambda) - r_i + 2r_{\text{H}} \ln \left(\frac{r(\lambda) - r_{\text{H}}}{r_i - r_{\text{H}}} \right) \right. \\ \left. + (r_{\text{H}}^2 + n^2) \left(\frac{1}{r_i - r_{\text{H}}} - \frac{1}{r(\lambda) - r_{\text{H}}} \right) \right). \quad (74)$$

Analogously in the case of the NUT–de Sitter and the charged NUT–de Sitter metrics with $r_{C-} < r_{H,i} < r_{H,o} < r_{C+}$ we obtain for $t_r(\lambda)$

$$t_r(\lambda) = i_{r_i} \frac{3}{\Lambda} \left(\frac{(r_{C+}^2 + n^2) \ln\left(\frac{r_{C+}-r_i}{r_{C+}-r(\lambda)}\right)}{(r_{C+}-r_{H,o})(r_{C+}-r_{H,i})(r_{C+}-r_{C-})} + \frac{(r_{H,o}^2 + n^2) \ln\left(\frac{r(\lambda)-r_{H,o}}{r_i-r_{H,o}}\right)}{(r_{C+}-r_{H,o})(r_{H,o}-r_{H,i})(r_{H,o}-r_{C-})} \right. \\ \left. + \frac{(r_{H,i}^2 + n^2) \ln\left(\frac{r_i-r_{H,i}}{r(\lambda)-r_{H,i}}\right)}{(r_{C+}-r_{H,i})(r_{H,o}-r_{H,i})(r_{H,i}-r_{C-})} + \frac{(r_{C-}^2 + n^2) \ln\left(\frac{r(\lambda)-r_{C-}}{r_i-r_{C-}}\right)}{(r_{C+}-r_{C-})(r_{H,o}-r_{C-})(r_{H,i}-r_{C-})} \right). \quad (75)$$

Finally for the extremally charged NUT–de Sitter metric with $r_{C-} < r_{H,i} = r_{H,o} = r_H < r_{C+}$ $t_r(\lambda)$ becomes

$$t_r(\lambda) = i_{r_i} \frac{3}{\Lambda} \left(\frac{(r_{C+}^2 + n^2) \ln\left(\frac{r_{C+}-r_i}{r_{C+}-r(\lambda)}\right)}{(r_{C+}-r_H)^2(r_{C+}-r_{C-})} + \frac{(r_{C+}^2 - r_{C-}^2)(r_H^2 - n^2) + 2r_H(r_{C+}(r_{C-}^2 + n^2) - r_{C-}(r_{C+}^2 + n^2))}{(r_{C+}-r_{C-})(r_{C+}-r_H)^2(r_H-r_{C-})^2} \ln\left(\frac{r(\lambda)-r_H}{r_i-r_H}\right) \right. \\ \left. + \frac{r_H^2 + n^2}{(r_{C+}-r_H)(r_H-r_{C-})} \left(\frac{1}{r_i-r_H} - \frac{1}{r(\lambda)-r_H} \right) + \frac{r_{C-}^2 + n^2}{(r_{C+}-r_{C-})(r_H-r_{C-})^2} \ln\left(\frac{r(\lambda)-r_{C-}}{r_i-r_{C-}}\right) \right). \quad (76)$$

Case 2: These are geodesics with $E^2/K > V_r(r_{ph-})$ and $K > 0$. They do not have turning points in the domain of outer communication. We perform a partial fraction decomposition of $\rho(r')^2/Q(r')$ and rewrite the right-hand side of Eq. (66) in terms of the elliptic integrals $t_{r,1}(r_i, r)$ and $t_{r,2}(r_i, r)$ given by Eqs. (A15) and (A16) in Appendix A 2 a. Now we substitute using Eq. (18) to rewrite the integrals in terms of Legendre's elliptic integral of the first kind and the two nonstandard elliptic integrals $G_L(\chi_i, \chi, k_1, n_k)$ and $H_L(\chi_i, \chi, k_1, n_k)$ given by Eqs. (A21) and (A22). We rewrite the latter in terms of elementary functions and Legendre's elliptic integrals of the first, second and third kind using Eqs. (A23)–(A25).

Case 3: These are geodesics with $E^2/K = V_r(r_{ph-})$. They have a double root at r_{ph-} and do not have turning points in the domain of outer communication. We first perform a partial fraction decomposition of $\rho(r')^2/Q(r')$. Then we perform a second partial fraction decomposition and restructure the right-hand side of Eq. (71) such that it only contains the elementary integrals $I_1 - I_5$ given by Eqs. (A1)–(A5) in Appendix A 1 a.

Case 4: These are geodesics with $V_r(r_{ph-}) > E^2/K > V_r(r_{ph})$. These geodesics have two real roots but no turning points in the domain of outer communication. Again we perform a partial fraction decomposition of $\rho(r')^2/Q(r')$. Then we use Eq. (28) to rewrite the right-hand side of Eq. (71) in terms of Legendre's elliptic integral of the first kind and the two nonstandard elliptic integrals $I_L(\chi_i, \chi, k_2, n_k)$ and $J_L(\chi_i, \chi, k_2, n_k)$. We rewrite $I_L(\chi_i, \chi, k_2, n_k)$ and $J_L(\chi_i, \chi, k_2, n_k)$ as Eqs. (A29), (A30), and (A32) as described in Appendix A 2 b.

Case 5: These are geodesics with $E^2/K = V_r(r_{ph})$. They either asymptotically come from or asymptotically go to the photon sphere at r_{ph} . Here we have to distinguish three

cases. In the first case we have $r(\lambda) = r_{ph}$. These are lightlike geodesics trapped on the photon sphere. Here, the right-hand side of Eq. (66) is constant. After a simple integration with respect to the Mino parameter $t_r(\lambda)$ now reads

$$t_r(\lambda) = \frac{\rho(r_{ph})^2 E(\lambda - \lambda_i)}{Q(r_{ph})}. \quad (77)$$

The other two cases only differ with respect to one term and an overall sign. In the first case we have $r_{H,o} < r < r_{ph}$ and in the second case we have $r_{ph} < r (< r_{C+})$. Again we first perform a partial fraction decomposition of $\rho(r')^2/Q(r')$. We substitute using Eq. (34) and subsequently perform a partial fraction decomposition with respect to y . Now we sort all terms such that only integrals given by $I_6 - I_9$ [Eqs. (A6)–(A9) in Appendix A 1 b] remain. Here, the main difference between $r_{H,o} < r < r_{ph}$ and $r_{ph} < r (< r_{C+})$ is that the term containing $1/(y - y_{ph})$ is given by I_6 [Eq. (A6)] for the former and by I_8 [Eq. (A8)] for the latter.

Case 6: These geodesics are characterized by $V_r(r_{ph}) > E^2/K$ and can have a turning point. For lightlike geodesics with $r_{H,o} < r < r_{ph}$ this turning point is always a maximum at $r_{max} = r_2$ and for $r_{ph} < r (< r_{C+})$ this turning point is always a minimum at $r_{min} = r_1$. Again we perform a partial fraction decomposition of $\rho(r')^2/Q(r')$. We substitute using Eq. (42) for $r_{H,o} < r < r_{ph}$ and Eq. (47) for $r_{ph} < r (< r_{C+})$. Now we sort all terms and rewrite them as Legendre's elliptic integrals of the first and third kind as well as the nonstandard elliptic integral $M_L(\chi_i, \chi, k_3, n_k)$. For the latter we now evoke Eq. (A34) in Appendix A 2 c to rewrite it in terms of elementary functions and

Legendre's elliptic integrals of the first, second and third kind.

IV. GRAVITATIONAL LENSING

A. Orthonormal tetrad and the angles on the observer's celestial sphere

The ultimate goal of theoretical predictions is to be verified by observations. In astronomy these observations are performed using telescopes on Earth's surface or in orbits around Earth. For astronomical observations it is a common standard to take the target of the observation as the center of the image and then divide the sky using a coordinate grid whose angular coordinates are measured from the target. Therefore, it will make our results much easier comparable to astronomical observations when we adapt this approach to our theoretical predictions. For achieving this goal we first introduce a stationary observer at coordinates $(x_O^\mu) = (t_O, r_O, \vartheta_O, \varphi_O)$ in the domain of outer communication between photon sphere and infinity or cosmological horizon for the (charged) NUT metric and the (charged) NUT–de Sitter metric, respectively. Here, the symmetries of the spacetimes allow us to set $t_O = 0$ and $\varphi_O = 0$. Now we choose the black hole as the target of our observation. In the next step we introduce an orthonormal tetrad e_0, e_1, e_2 , and e_3 as illustrated in Fig. 4 following the approach of Grenzebach *et al.* [39]:

$$e_0 = \sqrt{\frac{\rho(r)}{Q(r)}} \partial_t \Big|_{(x_O^\mu)}, \quad (78)$$

$$e_1 = \frac{1}{\sqrt{\rho(r)}} \partial_\vartheta \Big|_{(x_O^\mu)}, \quad (79)$$

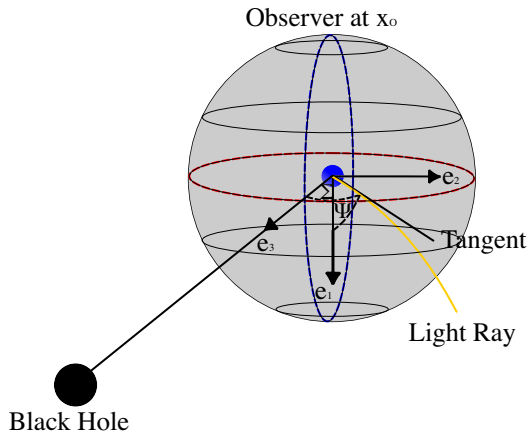


FIG. 4. Illustration of the lens-observer geometry and the orthonormal tetrad vectors e_1, e_2 and e_3 . The observer is located at $x_O = (x_O^\mu)$. A light ray is detected coming from the latitude Σ and the longitude Ψ on the observer's celestial sphere.

$$e_2 = -\frac{\partial_\varphi - 2n(\cos \vartheta + C)\partial_t}{\sqrt{\rho(r)} \sin \vartheta} \Big|_{(x_O^\mu)}, \quad (80)$$

$$e_3 = -\sqrt{\frac{Q(r)}{\rho(r)}} \partial_r \Big|_{(x_O^\mu)}, \quad (81)$$

where e_0 is the four-velocity vector of the observer. Now we introduce latitude and longitude coordinates Σ and Ψ such that the latitude Σ is measured from e_3 and the longitude Ψ is measured from e_1 in the direction of e_2 . In the next step we have to relate the three constants of motion E, L_z and K to the angular coordinates on the observer's celestial sphere. For this purpose let us consider the tangent vector of a light ray in Mino parametrization:

$$\frac{d\eta}{d\lambda} = \frac{dt}{d\lambda} \partial_t + \frac{dr}{d\lambda} \partial_r + \frac{d\vartheta}{d\lambda} \partial_\vartheta + \frac{d\varphi}{d\lambda} \partial_\varphi. \quad (82)$$

At the position of the observer we can also write the tangent vector of the light ray in terms of the orthonormal tetrad and the angles Σ and Ψ on the observer's celestial sphere as

$$\frac{d\eta}{d\lambda} = \sigma(-e_0 + \sin \Sigma \cos \Psi e_1 + \sin \Sigma \sin \Psi e_2 + \cos \Sigma e_3), \quad (83)$$

where σ is a normalization constant. In Mino parametrization the normalization constant σ is given by

$$\sigma = g\left(\frac{d\eta}{d\lambda}, e_0\right). \quad (84)$$

The Mino parameter is defined up to an affine transformation and therefore we can choose $\sigma = -\rho(r_O)$ without loss of generality. We insert σ and Eqs. (78)–(81) in Eq. (83) and compare coefficients with Eq. (82) evaluated at the position of the observer. Solving for E, L_z and K now leads to the following relations between the constants of motion E, L_z and K and the angles Σ and Ψ on the observer's celestial sphere:

$$E = \sqrt{\frac{Q(r_O)}{\rho(r_O)}}, \quad (85)$$

$$L_z = \sqrt{\rho(r_O)} \sin \vartheta_O \sin \Sigma \sin \Psi - 2n(\cos \vartheta_O + C) \sqrt{\frac{Q(r_O)}{\rho(r_O)}}, \quad (86)$$

$$K = \rho(r_O) \sin^2 \Sigma. \quad (87)$$

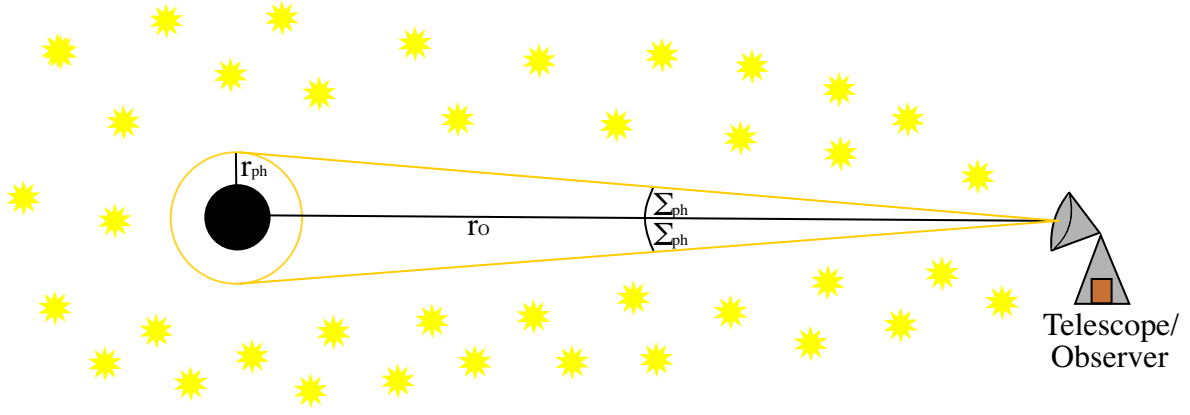


FIG. 5. Illustration of the construction of the shadow of a black hole. The black circle marks the region behind the horizon of the black hole. The yellow circle marks the photon sphere, the yellow stars are light sources and the yellow lines symbolize lightlike geodesics asymptotically coming from the photon sphere.

B. The shadow

When we consider gravitational lensing in a black hole spacetime one of the most easily accessible features is the shadow of the black hole. Although the shadow is a very idealized concept it is very characteristic and therefore in this section we calculate the angular radius of the shadow on the celestial sphere of an observer in the spacetime of a charged NUT–de Sitter black hole. For this purpose let us consider the same observer as in Sec. IV A fixed at coordinates (x_O^μ) . As illustrated in Fig. 5 we distribute light sources everywhere except between the black hole and the observer. The light sources are now associated with brightness on the observer’s celestial sphere while the void is associated with darkness on the observer’s celestial sphere. This dark area is the shadow of the black hole. The boundary between brightness and darkness exactly marks the direction of light rays asymptotically coming from the photon sphere. These light rays have exactly the same constants of motion as light rays on the photon sphere. In addition light rays asymptotically coming from the photon sphere have $dr/d\lambda|_{r=r_{\text{ph}}} = 0$. We now use this fact and the relations Eqs. (85) and (87) between the constants of motion E and K and the celestial latitude Σ to evaluate Eq. (6) at $r = r_{\text{ph}}$. We solve for $\Sigma = \Sigma_{\text{ph}}$ and obtain for the angular radius of the shadow of a charged NUT–de Sitter black hole

$$\Sigma_{\text{ph}} = \arcsin \left(\frac{\rho(r_{\text{ph}})}{\rho(r_o)} \sqrt{\frac{Q(r_o)}{Q(r_{\text{ph}})}} \right). \quad (88)$$

Note that this equation is structurally the same for all charged NUT–de Sitter metrics. The obtained result is already contained as special case in the results of Grenzebach *et al.* [31]; however, to our knowledge an explicit equation has not been derived yet. For $n \rightarrow 0$ Σ_{ph} reduces to the angular radius of the shadow of the Reissner–Nordström–de Sitter family of spacetimes:

$$\Sigma_{\text{ph},RNdS} = \arcsin \left(\frac{r_{\text{ph}}}{r_o} \sqrt{\frac{\tilde{Q}(r_o)}{\tilde{Q}(r_{\text{ph}})}} \right), \quad (89)$$

where $\tilde{Q}(r) = Q(r)/r^2$. In particular it reduces to Synge’s formula [45] for the Schwarzschild metric when $\Lambda \rightarrow 0$, $e \rightarrow 0$ and $n \rightarrow 0$. Although the charged NUT–de Sitter metric is only stationary and axisymmetric it is not surprising that the shadow is circular because of the metric’s $SO(3, \mathbb{R})$ symmetry. Figure 6 shows plots of the angular radius of the shadow Σ_{ph} as function of the gravitomagnetic charge n for the NUT metric (top left), the charged NUT metric with $e = 3m/4$ (top right), the NUT–de Sitter metric with $\Lambda = 1/(200m^2)$ (bottom left) and the charged NUT–de Sitter metric with $\Lambda = 1/(200m^2)$ and $e = 3m/4$ (bottom right) for $r_o = 4m$ (black solid), $r_o = 6m$ (blue dashed), $r_o = 8m$ (green dotted) and $r_o = 10m$ (red dashed-dotted). With increasing distance of the observer from the black hole Σ_{ph} decreases. In addition with increasing gravitomagnetic charge n the photon sphere expands and the angular radius of the shadow increases. For $r_{\text{ph}} \rightarrow r_o$ we have $\Sigma_{\text{ph}} \rightarrow \pi/2$ and the shadow covers half of the observer’s sky. For $r_{\text{H},o} < r_o < r_{\text{ph}}$ (not shown) the complement of the shadow, usually also referred to as escape cone, shrinks while r_o approaches the outer black hole horizon $r_{\text{H},o}$. When we turn on the electric charge e (top right) the angular radius of the shadow shrinks slightly because in the presence of the electric charge r_{ph} is slightly smaller. As a consequence Σ_{ph} approaches $\pi/2$ for larger n . Something similar happens when we turn on the cosmological constant Λ . We can see in the bottom panels that for $\Lambda > 0$ the angular radius of the shadow Σ_{ph} also slightly decreases. With increasing n the photon sphere expands and r_{ph} approaches r_o slightly faster than for the NUT metric and the charged NUT metric. As a consequence Σ_{ph} approaches $\pi/2$ for slightly smaller gravitomagnetic charges n . However, unlike for the Schwarzschild–de Sitter and the Reissner–Nordström–de

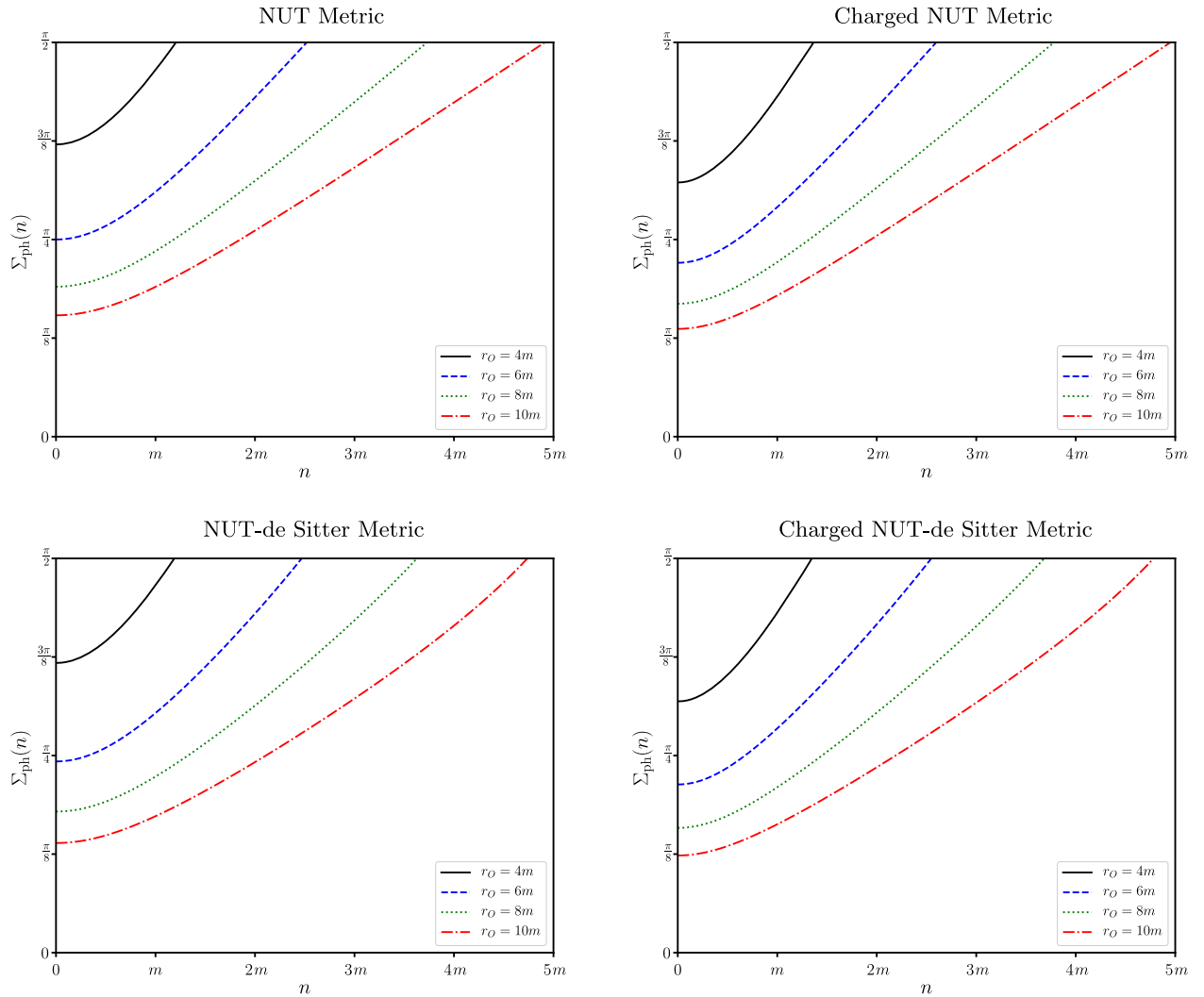


FIG. 6. Angular radius of the shadow Σ_{ph} for observers at radii $r_O = 4m$ (black), $r_O = 6m$ (blue dashed), $r_O = 8m$ (green dotted) and $r_O = 10m$ (red dashed-dotted) for the NUT metric (top left), the charged NUT metric with $e = 3m/4$ (top right), the NUT-de Sitter metric with $\Lambda = 1/(200m^2)$ (bottom left), and the charged NUT-de Sitter metric with $\Lambda = 1/(200m^2)$, $e = 3m/4$ (bottom right).

Sitter metrics, for which the radius coordinate r_{ph} of the photon sphere is independent of the cosmological constant, we cannot only attribute these effects to Eq. (88) but also have to consider the effect of the cosmological constant on the radius coordinate of the photon sphere r_{ph} itself [as determined from Eq. (12)]. As discussed in Sec. III A 1 when we turn on the cosmological constant Λ the photon sphere expands much faster for increasing n compared to $\Lambda = 0$ and this effect gets stronger the larger the gravitomagnetic charge n . This leads to the observed fact that Σ_{ph} approaches $\pi/2$ already for smaller n .

In this paper we only considered stationary observers. So the immediate question arises how the shadow would look like for an observer moving at a constant velocity v . Here, we can draw insight by having a look at the reasoning of Penrose [46] on the appearance of a moving sphere to a resting observer. For a resting observer a

moving sphere always appears to be circular independent of how it moves relative to the observer. Now we can always find a coordinate system in which the observer is moving relative to the resting sphere. In the new coordinate system the sphere is at rest while the observer moves. Therefore, both a resting observer and a moving observer see a sphere as a circle on their skies. We can now immediately transfer this reasoning to the shadow. The photon sphere takes the role of the sphere and the shadow is seen by a distant observer as a circle of darkness. The angular radius of the shadow on the celestial sphere of the moving observer can then be calculated from the angular radius of the shadow on the celestial sphere of the resting observer by applying the aberration formula. Because the aberration formula maps circles on circles the shadow is circular for both the resting and the moving observers.

How can we now use our insights to measure the gravitomagnetic charge from observations of the shadow? As discussed above the gravitomagnetic charge n affects the size of the shadow. Even if the gravitomagnetic charge is only very small it will lead to a larger angular radius Σ_{ph} of the shadow compared to a spacetime without gravitomagnetic charge. However, as we can read from Eqs. (88) and (89) as long as we have vanishing spin the shadow is always circular independent of the presence of the gravitomagnetic charge. To make things worse also observers around black holes potentially described by the charged C–de Sitter metrics, which describe charged accelerating black holes with a cosmological constant, see a circular shadow [38,42]. While it is true that the angular radius of the shadow in the C–de Sitter metrics decreases with increasing acceleration parameter as the observer approaches the acceleration horizon, in reality we can expect both, the acceleration parameter and the gravitomagnetic charge and also their effects on the shadow to be very small. Therefore even if we only consider the Plebański-Demiański class we have a degeneracy between 12 spacetimes that can potentially describe black holes with circular shadows in nature. Because we do not *a priori* know the distance between Earth and an observed astrophysical black hole we cannot lift this degeneracy using observations of the shadow alone. Mars *et al.* [47] showed that for Kerr-Newman black holes and observers that are not located on the axis of symmetry this degeneracy is lifted. They also concluded that for Kerr-Newman-NUT black holes the only parameter that cannot be determined from observations of the shadow alone is the gravitomagnetic charge n . However, in this paper we do not consider the spin and therefore we need additional observables that help us to distinguish between the shadows in different spacetimes and to potentially measure the gravitomagnetic charge n .

C. The lens equation

We now move on to define the lens map. The most general version of a general relativistic lens map was first introduced by Frittelli and Newman [48] and later adapted to spherically symmetric spacetimes by Perlick [49]. Only recently the approach of Perlick was adapted to axisymmetric spacetimes in Frost and Perlick [38] and Frost [42]. We now apply their approach to the charged NUT–de Sitter metrics. For this purpose we proceed as follows.

We first distribute light sources on a two-sphere S_L^2 at the radius coordinate r_L . We place the stationary observer with coordinates (x_O^μ) at a radius coordinate $r_{\text{ph}} < r_O < r_L (< r_{C+})$ and construct its past light cone. We follow all lightlike geodesics on this cone back into the past. Some of these geodesics will intersect with the two-sphere S_L^2 while others will intersect with the outer black hole horizon $r_{\text{H},0}$ and end up in the black hole. The geodesics that intersect with the two-sphere S_L^2 now constitute a map from the

celestial coordinates Σ and Ψ on the celestial sphere of the observer to the angular coordinates $\vartheta_L(\Sigma, \Psi)$ and $\varphi_L(\Sigma, \Psi)$ on the two-sphere of light sources S_L^2 :

$$(\Sigma, \Psi) \rightarrow (\vartheta_L(\Sigma, \Psi), \varphi_L(\Sigma, \Psi)). \quad (90)$$

This is our lens equation. For the calculation of the lens map we now employ the solutions for $\vartheta(\lambda)$ and $\varphi(\lambda)$ calculated in Secs. III B and III C. We express the constants of motion in Eqs. (55), (56), and (61)–(64) by Eqs. (85)–(87). Now we choose $\lambda_O = 0$ and thus the only thing left to do is to eliminate the unknown $\lambda_L < \lambda_O$. We can calculate it from the radius coordinates of the observer r_O and the radius coordinate r_L at which the light ray intersects with the two sphere S_L^2 . For this purpose we separate variables in Eq. (6) and integrate. Now we have to distinguish two different types of lightlike geodesics. The first type of lightlike geodesics has a turning point at the radius coordinate $r_{\text{min}} = r_1$. In this case λ_L becomes

$$\lambda_L = \int_{r_O}^{r_{\text{min}}} - \int_{r_{\text{min}}}^{r_L} \frac{\sqrt{\rho(r_O)} dr'}{\sqrt{\rho(r')^2 Q(r_O) - Q(r') \rho(r_O)^2 \sin^2 \Sigma}}. \quad (91)$$

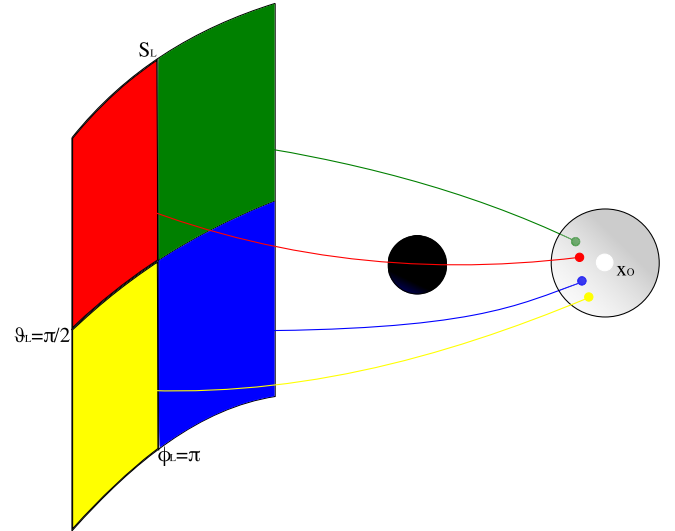


FIG. 7. A simple illustration of the lens map. The black sphere in the center represents the black hole. The white dot and the gray area surrounding it are the observer and their celestial sphere at $x_O = (x_O^\mu)$. The colored area represents a patch on the two-sphere of light sources S_L^2 with coordinate radius r_L . The two-sphere S_L^2 is colored using the convention in Bohn *et al.* [51]. Extended to the whole sphere we color it as follows: $0 \leq \vartheta_L \leq \pi/2$ and $0 \leq \varphi_L < \pi$: green, $\pi/2 < \vartheta_L \leq \pi$ and $0 \leq \varphi_L < \pi$: blue, $0 \leq \vartheta_L \leq \pi/2$ and $\pi \leq \varphi_L < 2\pi$: red, $\pi/2 < \vartheta_L \leq \pi$ and $\pi \leq \varphi_L < 2\pi$: yellow. The colored lines represent lightlike geodesics emitted by light sources on each patch of the two-sphere S_L^2 .

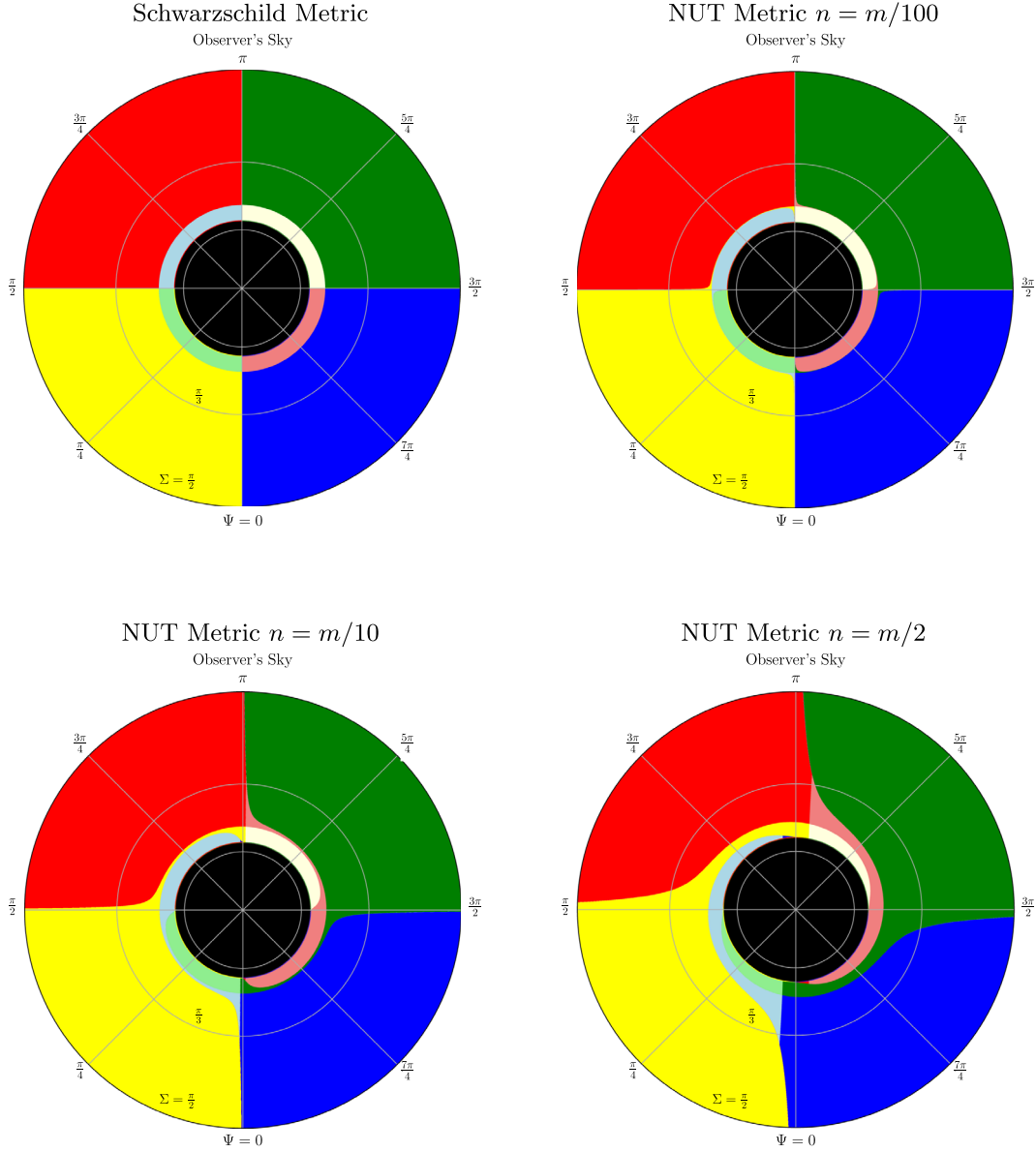


FIG. 8. Lens maps for light rays emitted by light sources located on the two-sphere S_L^2 at the radius coordinate $r_L = 9m$ and detected by an observer located at $r_O = 8m$, $\vartheta_O = \pi/2$ in the Schwarzschild metric (top left) and in the NUT metric with $n = m/100$ (top right), $n = m/10$ (bottom left), and $n = m/2$ (bottom right). The Misner string is located at $\vartheta = 0$ ($C = 1$).

The second type of lightlike geodesics does not have a turning point and is propagating in the radial direction outward. In this case λ_L reads

$$\lambda_L = - \int_{r_O}^{r_L} \frac{\sqrt{\rho(r_O)} dr'}{\sqrt{\rho(r')^2 Q(r_O) - Q(r') \rho(r_O)^2 \sin^2 \Sigma}}. \quad (92)$$

For the calculation of the lens map we now rewrite λ_L in terms of Legendre's elliptic integral of the first kind or when possible in terms of elementary functions. We calculate $\vartheta_L(\Sigma, \Psi)$ and $\varphi_L(\Sigma, \Psi)$ as described in Secs. III B and III C. For a fast and efficient calculation

of the lens equation and the travel time in Sec. IV E their evaluation was implemented in the programming language JULIA [50]. For the visual representation we follow the color conventions of Bohn *et al.* [51] illustrated in Fig. 7 with a small modification which will be described below.

Figure 8 shows the lens map for an observer located at $r_O = 8m$ and $\vartheta_O = \pi/2$ and a sphere of light sources S_L^2 at the radius coordinate $r_L = 9m$ for the Schwarzschild metric (top left), the NUT metric with $n = m/100$ (top right), $n = m/10$ (bottom left) and $n = m/2$ (bottom right). The Misner string is located at $\vartheta = 0$ ($C = 1$). The observer looks in the direction of the black hole. The black circle in the center is the shadow of the black hole. In the

Schwarzschild metric the lens map is rotationally symmetric. The rings around the center represent images of different orders. Here, we say that an image is of order n_{im} when the absolute value of the covered angle $\Delta\varphi_L$ fulfills the relation $(n_{\text{im}} - 1)\pi < |\Delta\varphi_L| < n_{\text{im}}\pi$. The outer, strongly colored ring represents images of first order, while the second, fainter colored ring represents images of second order. Closer to the shadow we can also see images of third and, when we zoom in, images of fourth order. The borders between the images of different orders are the critical curves. Patches with the same color represent images from light sources on the same quadrant on the sphere of light sources. In our representation we slightly deviate from the representation of Bohn *et al.* [51] as we represent images of odd order by stronger colors than images of even order. When we now turn on the gravitomagnetic charge n the patches on the observer's sky start to become twisted and the formerly separated areas in the rings with images of first and second order connect. This effect becomes stronger the larger the gravitomagnetic charge n . The pattern of the lens map is symmetric under rotations by π . The images of first and second order from the same quadrant on the two-sphere S_L^2 are separated by sharp lines. The geodesics exactly on these lines cross the axes at least once (here we have to note that these geodesics can only cross one axis, either $\vartheta = 0$ or $\vartheta = \pi$). In the lower two panels we also observe odd order images close to the shadow at $\Psi = 0$ (red) and $\Psi = \pi$ (blue). A closer investigation reveals that formally these are images of first order. The associated lightlike geodesics move on cones not enclosing the axes and thus along these geodesics the direction of the φ motion reverses. Considering the observed lensing pattern it is now an interesting question how the critical curves of the NUT metric look. In Fig. 9 we show an enlarged view of the lens map between $\Psi = \pi$ and $\Psi = 9\pi/8$ for the NUT metric with $n = m/2$ with 16 times higher Ψ resolution than for Fig. 8. The sharp boundaries still remain and therefore we can exclude with high certainty that they are artifacts of too-scarce point sampling. However, although these lines separate images of first and second order it is rather unlikely that they are part of the critical curves for three reasons. First of all, although not clearly visible in the top right panel of Fig. 8 they form as soon as we turn on the gravitomagnetic charge n . As discussed above for the Schwarzschild metric the critical curves are circles and *a priori* there seems to be no reason why this should suddenly change. Second, the NUT metric maintains an $SO(3, \mathbb{R})$ symmetry which also strongly suggests that the critical curves are likely to be circles. Third, if we have a closer look images of first and second order and images of third and fourth order seem to be clearly separated by circles indicating that this boundary is a critical curve. Settling this question would require a more detailed analysis of the geodesic motion in the NUT metric or exactly deriving the determining relation for the critical

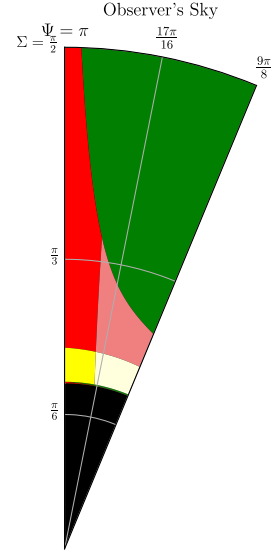


FIG. 9. Enlarged view of the lens map in Fig. 8 (bottom right) between $\Psi = \pi$ and $\Psi = 9\pi/8$ for light rays emitted by light sources located on the two-sphere S_L^2 at the radius coordinate $r_L = 9m$ and detected by an observer located at $r_O = 8m$, $\vartheta_O = \pi/2$ in the NUT metric with $n = m/2$. The Misner string is located at $\vartheta = 0$ ($C = 1$).

curves. Both are beyond the scope of this paper and will be part of future work. Figure 10 shows the lens maps of the Reissner-Nordström metric (top left), the charged NUT metric (top right), the Schwarzschild–de Sitter metric (middle left), the NUT–de Sitter metric (middle right), the Reissner-Nordström–de Sitter metric (bottom left) and the charged NUT–de Sitter metric (bottom right) with $\Lambda = 1/(200m^2)$, $e = 3m/4$ and $n = m/2$ in the respective cases for an observer at $r_O = 8m$ and $\vartheta_O = \pi/2$ and light sources distributed on the two-sphere S_L^2 with radius coordinate $r_L = 9m$. The Misner string is located at $\vartheta = 0$ ($C = 1$). As soon as we turn on the electric charge e and the cosmological constant Λ the shadow shrinks; however, the overall pattern of the lens map remains the same.

The twist observed in Figs. 8 and 10 has already been observed by Lynden-Bell and Nouri-Zonoz [16,26] in the weak-field limit. When we observe a circular shadow this is one of two recognizable characteristics indicating the presence of the gravitomagnetic charge n . This twist can potentially be observed when we observe multiple images from light sources at approximately the same distance from the black hole, e.g., in a star cluster or a galaxy cluster. Identifying enough images and their positions on the sky will allow us to construct a partial lens map and potentially infer the magnitude of the twist. From the determined magnitude of the twist we can then draw conclusions on the magnitude of the gravitomagnetic charge n . Although this partial lens map may allow us to draw conclusions on the presence and potentially the magnitude of the gravitomagnetic charge n it will not allow us to lift the degeneracy with

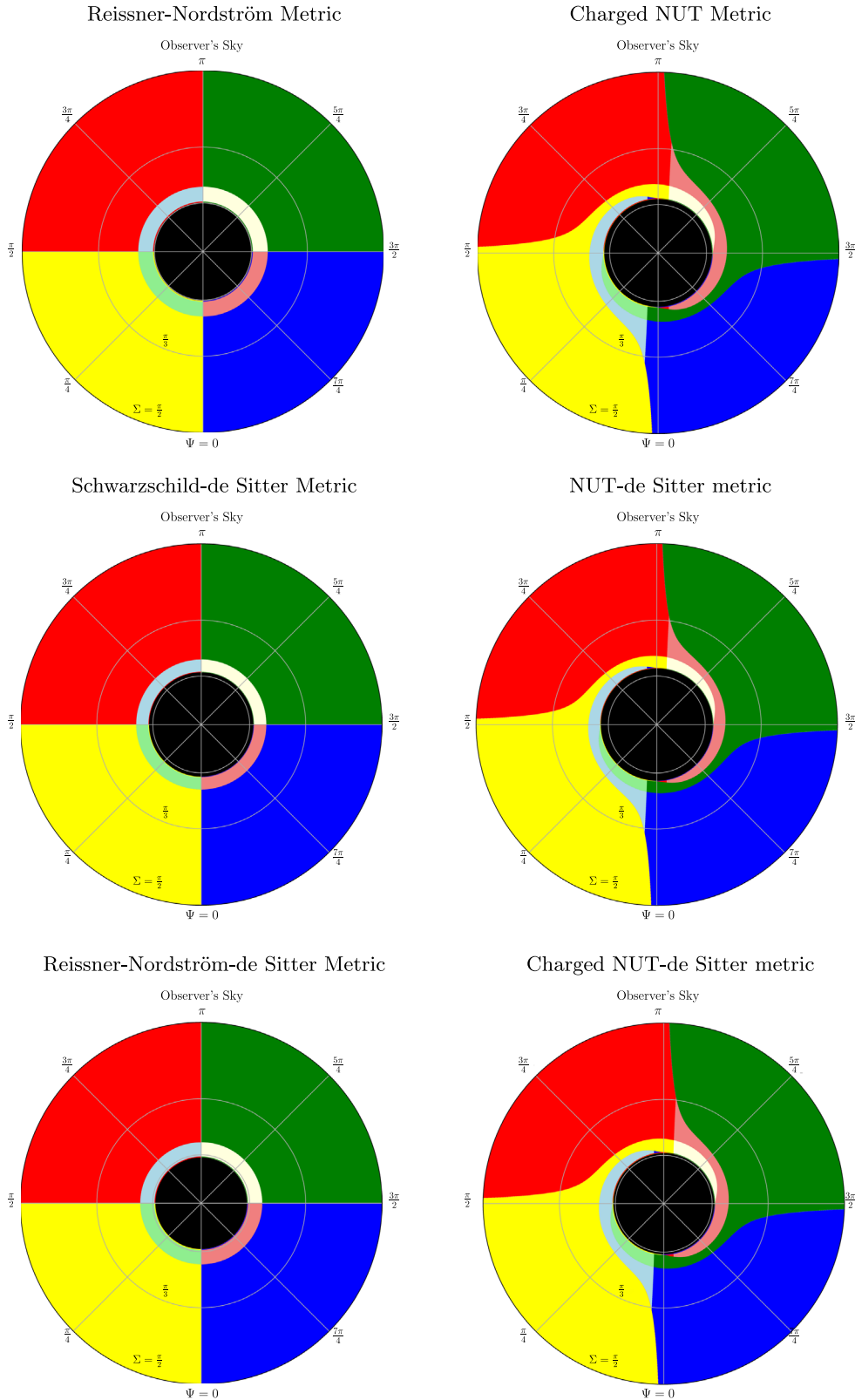


FIG. 10. Lens maps for light rays emitted by light sources located on the two-sphere S_L^2 at the radius coordinate $r_L = 9m$ and detected by an observer located at $r_O = 8m$, $\vartheta_O = \pi/2$, in the Reissner-Nordström metric (top left), the charged NUT metric (top right), the Schwarzschild-de Sitter metric (middle left), the NUT-de Sitter metric (middle right), the Reissner-Nordström-de Sitter metric (bottom left), and the charged NUT-de Sitter metric (bottom right). The cosmological constant Λ , the electric charge e and the gravitomagnetic charge n are $\Lambda = 1/(200m^2)$, $e = 3m/4$, and $n = m/2$, respectively. The Misner string is located at $\vartheta = 0$ ($C = 1$).

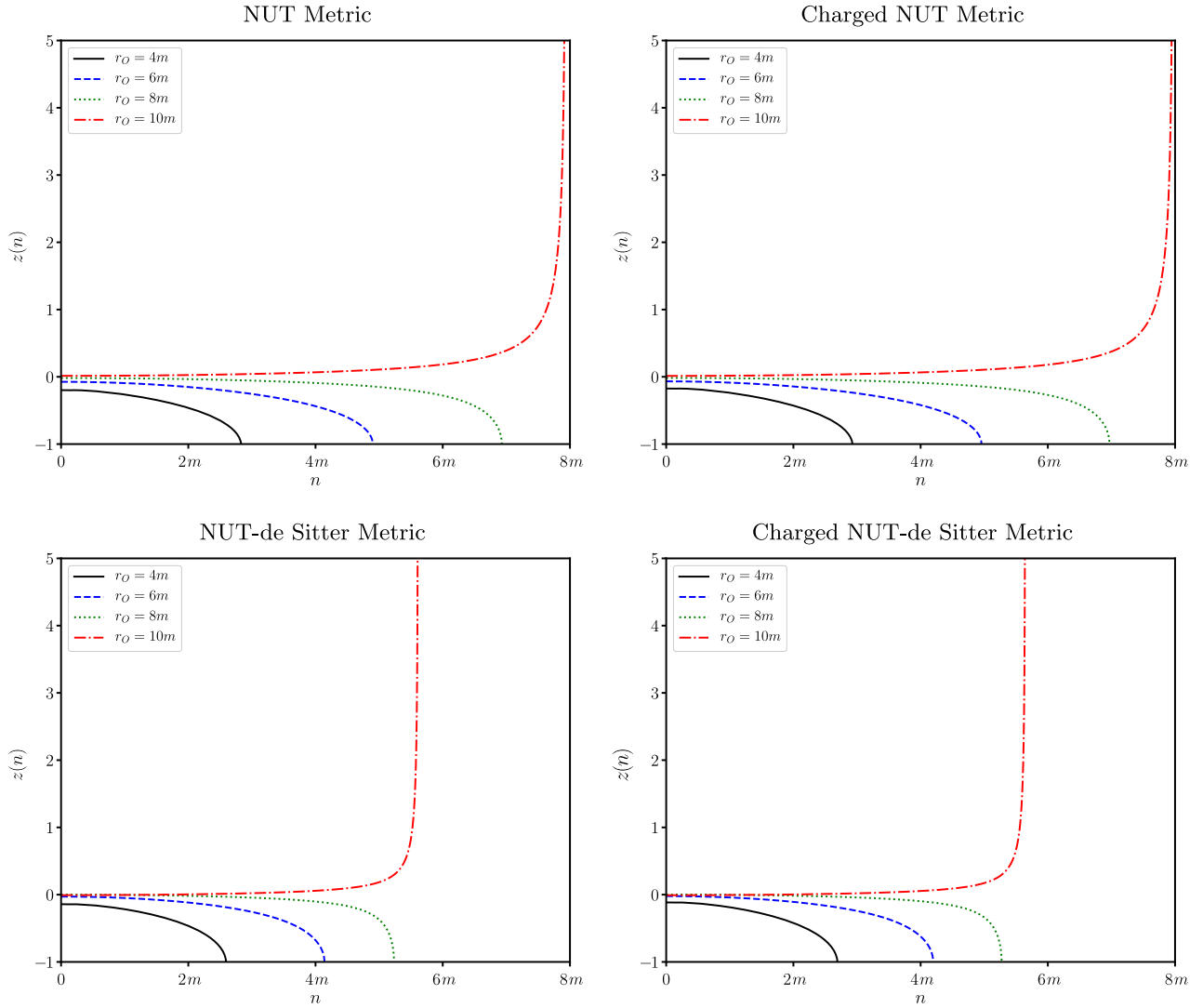


FIG. 11. Redshift for observers at radii $r_O = 4m$ (black), $r_O = 6m$ (blue dashed), $r_O = 8m$ (green dotted), and $r_O = 10m$ (red dashed-dotted) and a light source at $r_L = 9m$ for the NUT metric (top left), the charged NUT metric with $e = 3m/4$ (top right), the NUT–de Sitter metric with $\Lambda = 1/(200m^2)$ (bottom left) and the charged NUT–de Sitter metric with $\Lambda = 1/(200m^2)$, $e = 3m/4$ (bottom right).

respect to the cosmological constant Λ , the electric charge e , r_O and r_L .

D. Redshift

The redshift factor z measures the relative energy shift that a light ray experiences on its way from the light source by which it was emitted to the observer by whom it is detected. It is one of the few observables that is directly accessible to observations and can be determined by comparing the measured frequencies of known emission lines in the emission spectrum of, e.g., a star, to their unshifted frequencies from, e.g., laboratory measurements. In our case the observer as well as the light source are stationary and since we do not consider spinning black holes both move on t lines. For this emitter-observer constellation the redshift factor z is thoroughly derived,

e.g., in the book of Straumann [52], pp. 45. In terms of the metric coefficients it reads

$$z = \sqrt{\frac{g_{tt}|_{x_O}}{g_{tt}|_{x_L}}} - 1. \tag{93}$$

Now we insert the metric coefficient $g_{tt} = -Q(r)/\rho(r)$ and get z in terms of the spacetime coordinates:

$$z = \sqrt{\frac{\rho(r_L)Q(r_O)}{\rho(r_O)Q(r_L)}} - 1. \tag{94}$$

For the charged NUT–de Sitter spacetimes z only depends on the radius coordinates r_O of the observer and r_L of the light source and the four parameters m , Λ , e and n . Figure 11 shows the redshift factor z for observers at

radius coordinates $r_O = 4m$, $r_O = 6m$, $r_O = 8m$, and $r_O = 10m$ and a light source at the radius coordinate $r_L = 9m$ as function of the gravitomagnetic charge n for the NUT metric (top left), the charged NUT metric (top right), the NUT–de Sitter metric (bottom left) and the charged NUT–de Sitter metric (bottom right). The cosmological constant and the electric charge are $\Lambda = 1/(200m^2)$ and $e = 3m/4$, respectively. For $n = 0$ the redshift factor z reduces to the redshift factors in the Schwarzschild metric (top left), the Reissner-Nordström metric (top right), the Schwarzschild–de Sitter metric (bottom left) and the Reissner-Nordström–de Sitter metric (bottom right), respectively.

For $r_O < r_L$ we mainly have blueshifts while for $r_L < r_O$ we mainly have redshifts. When we now turn on the gravitomagnetic charge n in the former case with growing gravitomagnetic charge the outer black hole horizon approaches the observer $r_{H,o} \rightarrow r_O$ and thus light rays emitted by the light source are infinitely blueshifted leading to $z \rightarrow -1$. In the latter case with growing gravitomagnetic charge n the outer black hole horizon approaches the light source $r_{H,o} \rightarrow r_L$ and thus light rays emitted by this source become infinitely redshifted and we have $z \rightarrow \infty$.

When we now turn on the electric charge e for small $n \approx 0$ the blueshifts and the redshifts slightly decrease. The outer black hole horizon is originally located at a smaller radius coordinate and thus we have $z \rightarrow -1$ and $z \rightarrow \infty$ for slightly larger gravitomagnetic charges n , respectively. Turning on the cosmological constant Λ has a similar effect. The outer black hole horizon is originally located at a slightly larger radius coordinate $r_{H,o}$ and expands faster with increasing n . Therefore we have $z \rightarrow -1$ and $z \rightarrow \infty$ for much smaller gravitomagnetic charges n .

For observations it is rather unfortunate that in addition to the four parameters m , Λ , e and n the redshift factor z only depends on the radius coordinates of the observer r_O and of the light source r_L . While the redshift factor z is also

affected by the gravitomagnetic charge n this information is useless as long as we do not *a priori* know the distances between observer and black hole and light source and black hole. Therefore, similar to the angular radius of the shadow, we have a degeneracy between the redshift factors in spherically symmetric spacetimes and the charged NUT–de Sitter metrics for different cosmological constants Λ , electric charges e , gravitomagnetic charges n , r_O , and r_L . However, combined with information about the angular radius of the shadow Σ_{ph} , from the lens equation and travel-time differences (these will be discussed in the next section) there is a chance that we can lift this degeneracy and determine Λ , e , and n .

E. Travel time

The travel time T measures in terms of the time coordinate t the time a light ray needs to travel from the light source by which it was emitted to an observer by whom it is detected. For a light ray that is emitted at the time coordinate t_L and detected by an observer at the time coordinate t_O it reads

$$T = t_O - t_L. \quad (95)$$

The travel time is not directly measurable; however, in the case that we can identify multiple images of the same light source, e.g., a quasar (see Fohlmeister *et al.* [53] or Koptelova *et al.* [54]) we can record light curves for each image and compare their variability. When we are able to identify similar structures we can now determine the time delay between the images.

We now want to construct travel-time maps for the charged NUT–de Sitter spacetimes. For this purpose we now insert Eqs. (85)–(87) in Eq. (65) and rewrite it with the help of Eq. (6) as (remember that we set $t_O = 0$)

$$T(\Sigma, \Psi) = \int_{r_O \dots}^{\dots r_L} \frac{\sqrt{Q(r_O)} \rho(r')^2 dr'}{Q(r') \sqrt{\rho(r')^2 Q(r_O) - Q(r') \rho(r_O)^2} \sin^2 \Sigma} - 2n \int_0^{\lambda_L} (\cos \vartheta(\lambda') + C) \frac{\left(\sqrt{\rho(r_O)} \sin \vartheta_O \sin \Sigma \sin \Psi + 2n (\cos \vartheta(\lambda') - \cos \vartheta_O) \sqrt{\frac{Q(r_O)}{\rho(r_O)}} \right) d\lambda'}{1 - \cos^2 \vartheta(\lambda')}. \quad (96)$$

The dots in the limits of the integral of the first term shall indicate that we have to split the integral at the turning point. For observers between photon sphere and infinity ($\Lambda = 0$) or the cosmological horizon ($0 < \Lambda < \Lambda_C$) this is always a minimum. In the same term the sign of the root has to be chosen such that it agrees with the direction of the r motion along the geodesic. We now rewrite the term in terms of elementary functions and Legendre’s elliptic integrals of the first, second and third kind as described

in Sec. III D 2. Analogously we integrate the second term on the right-hand side following the steps described in Sec. III D 1.

For a fast and efficient evaluation the calculation of the travel time was implemented in JULIA using the same set of program routines as for the lens equation.

Figure 12 shows the travel time in the Schwarzschild metric (top left) and the NUT metric with a Misner string at $\vartheta = 0$ ($C = 1$) and $n = m/100$ (top right), $n = m/10$

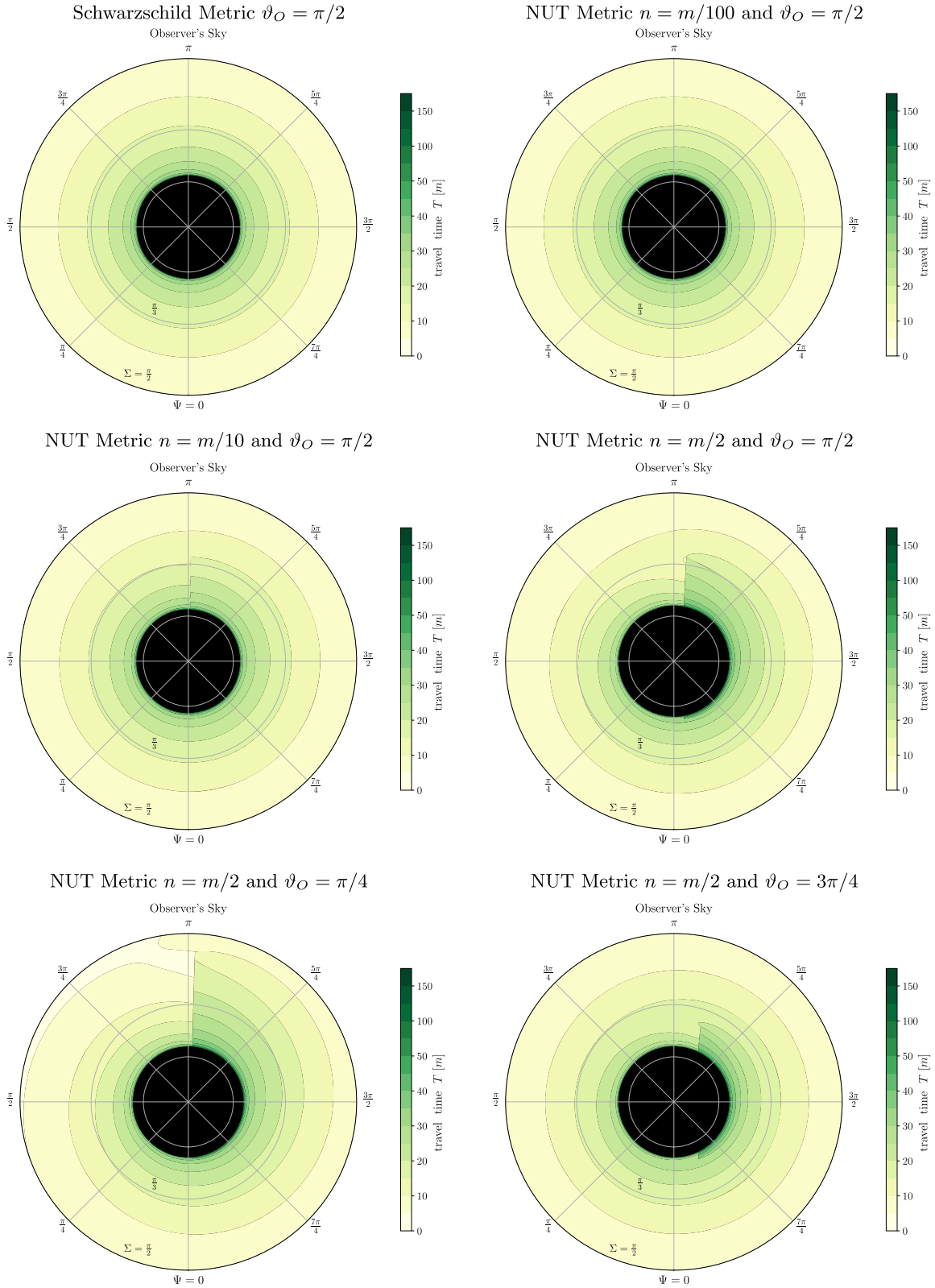


FIG. 12. Travel-time maps for light rays emitted by light sources located on the two-sphere S_L^2 at the radius coordinate $r_L = 9m$ and detected by an observer located at $r_O = 8m$ and $\vartheta_O = \pi/2$ in the Schwarzschild metric (top left) and the NUT metric with $n = m/100$ (top right), $n = m/10$ (middle left) and $n = m/2$ (middle right) and two observers located at $\vartheta_O = \pi/4$ (bottom left) and $\vartheta_O = 3\pi/4$ (bottom right) in the NUT metric with $n = m/2$. The Misner string is located at $\vartheta = 0$ ($C = 1$).

(middle left) and $n = m/2$ (middle right) for an observer located at $r_O = 8m$ and $\vartheta_O = \pi/2$. In addition it also shows travel-time maps for observers located at $r_O = 8m$ and $\vartheta_O = \pi/4$ (bottom left) and $\vartheta_O = 3\pi/4$ (bottom right) in the NUT spacetime with $n = m/2$. The light sources are located on the two-sphere S_L^2 at the radius coordinate $r_L = 9m$. The travel time increases towards the shadow as the light ray makes more and more turns around the black hole. For the Schwarzschild metric (top left) the travel time is rotationally symmetric under arbitrary rotations about the axis $\Sigma = 0$. For $n = m/100$ (top right) the travel time shows still a high degree of apparent rotational symmetry. When we look closer, however, we can recognize an apparent sharp discontinuity at $\Psi = \pi$. When we increase the gravitomagnetic charge n this discontinuity becomes more and more pronounced. When we start at the discontinuity and go in clockwise direction along a constant latitude Σ the travel time decreases. In the travel-time maps this decrease forms the shape of a spiral. In addition with increasing n a second discontinuity starts to become visible on the right-hand side of $\Psi = 0$ close to the shadow. When we zoom in on the middle right panel of Fig. 12 we recognize that the first discontinuity consists of very narrow steps and thus from this map alone it is unclear if this is a real sharp discontinuity or if the travel time simply shows a very steep increase. In all three panels these discontinuities appear exactly for lightlike geodesics crossing the Misner string. Figure 13 shows an enlarged view of the discontinuity close to $\Psi = \pi$ between $\Psi = \pi$ and $\Psi = 9\pi/8$ for $n = m/2$ with a 16 times higher Ψ resolution than in the

middle right panel of Fig. 12. The figure clearly shows that the travel time has a real discontinuity for lightlike geodesics crossing the Misner string. From the observer's perspective lightlike geodesics passing to the left of the Misner string have a shorter travel time than light rays passing to the right of the Misner string. When the observer moves to lower spacetime latitudes ϑ the discontinuity of the travel time close to $\Psi = \pi$ stretches out to higher latitudes Σ on the observer's celestial sphere while the discontinuity close to $\Psi = 0$ is confined to a much more narrow region close to the shadow. In addition compared to an observer at $\vartheta_O = \pi/2$ for the observer at $\vartheta_O = \pi/4$ they appear closer to $\Psi = \pi$ and $\Psi = 0$, respectively. For an observer at $\vartheta_O = 3\pi/4$ the situation is reversed. The discontinuity at $\Psi = \pi$ becomes more confined to the shadow while the discontinuity at $\Psi = 0$ can already be observed at higher latitudes Σ . In addition both discontinuities can be found at longitudes Ψ further away from $\Psi = \pi$ and $\Psi = 0$, respectively.

Figures 14–16 show the travel-time maps for observers in the Reissner-Nordström metric (Fig. 14, top left), the Schwarzschild-de Sitter metric (Fig. 15, top left), the Reissner-Nordström-de Sitter metric (Fig. 16, top left), the charged NUT metric (Fig. 14, top right and bottom row), the NUT-de Sitter metric (Fig. 15, top right and bottom row) and the charged NUT-de Sitter metric (Fig. 16, top right and bottom row) for observers located at the radius coordinate $r_O = 8m$ and the spacetime latitudes $\vartheta_O = \pi/4$ (only for $n > 0$), $\vartheta_O = \pi/2$ and $\vartheta_O = 3\pi/4$ (only for $n > 0$). The two-sphere S_L^2 is located at the radius coordinate $r_L = 9m$. The electric charge and the cosmological constant are $e = 3m/4$ and $\Lambda = 1/(200m^2)$, respectively. When we turn on the electric charge e (Fig. 14) the shadow shrinks and the travel time shows roughly the same pattern just shifted to lower latitudes. When we turn on the cosmological constant (Figs. 15 and 16) the area of the shadow shrinks while we observe an overall increase of the travel time. However, like after turning on the electric charge except for some minor details the overall patterns on the travel-time maps remain the same.

The travel time just provided us with a second unique pattern that indicates the presence of a gravitomagnetic charge. When a black hole has a gravitomagnetic charge and when it is described by one of the charged NUT-de Sitter metrics we will observe a discontinuity whenever light rays cross the Misner strings. While the Misner strings are very likely only mathematical idealizations of a real physical effect and thus in reality it is more likely that we will observe a transition from shorter to longer travel times (or vice versa) this effect may still be observable.

As stated above we *cannot* observe absolute travel times of light rays but only travel-time differences. Considering the uniqueness of the discontinuity the best chance to

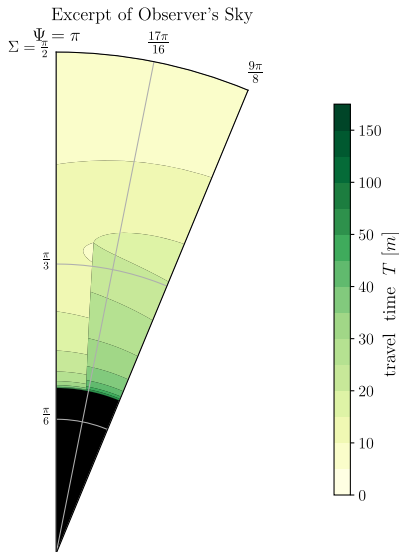


FIG. 13. Enlarged view of the travel-time map in Fig. 12 (middle right) between $\Psi = \pi$ and $\Psi = 9\pi/8$ for light rays emitted by light sources located on the two-sphere S_L^2 at the radius coordinate $r_L = 9m$ and detected by an observer located at $r_O = 8m$, $\vartheta_O = \pi/2$ in the NUT metric with $n = m/2$. The Misner string is located at $\vartheta = 0$ ($C = 1$).

observe it would be the use of quadruply lensed stars or quasars. When we observe lensed images of these sources more or less forming a cross around the lens (see, e.g., Suyu *et al.* [55]) we can determine travel-time differences between the images. In the case they are at roughly the

same distance from the black hole and have roughly the same angular distance from each other (like, e.g., for HE 0435-1223 in Fig. 1 of Suyu *et al.* [55]) the observed discontinuity in the travel time will lead to a high travel-time difference between the images with the smallest

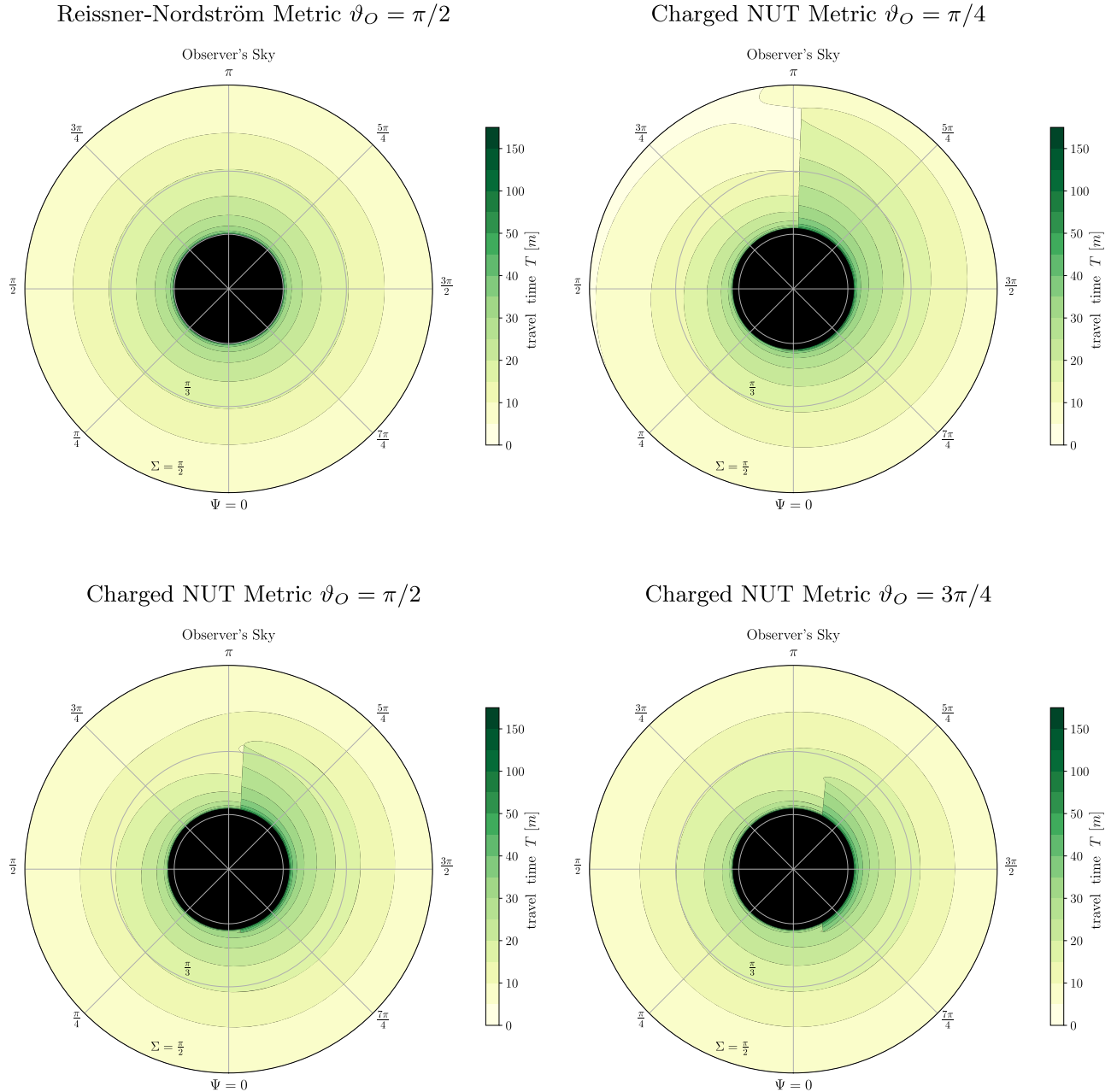


FIG. 14. Travel-time maps for light rays emitted by light sources located on the two-sphere S_L^2 at the radius coordinate $r_L = 9m$ and detected by an observer located at $r_O = 8m$ and $\vartheta_O = \pi/2$ in the Reissner-Nordström metric (top left), $\vartheta_O = \pi/4$ (top right), $\vartheta_O = \pi/2$ (bottom left), and $\vartheta_O = 3\pi/4$ (bottom right) in the charged NUT metric with $n = m/2$. The electric charge is $e = 3m/4$. The Misner string is located at $\vartheta = 0$ ($C = 1$).

angular distances to the discontinuity while the travel-time difference between the other images will be much smaller. The travel-time difference may allow to distinguish black holes with gravitomagnetic charge n from black holes without gravitomagnetic charge but it does not allow to lift the degeneracy with respect to Λ , e , r_O , and r_L .

Unfortunately so far we did not observe quadruply imaged stars lensed by black holes. Indeed, so far light sources multiply imaged by black holes were not observed at all and thus we will have to wait until the next generations of telescopes become available that have a resolution that is high enough to address this challenge.

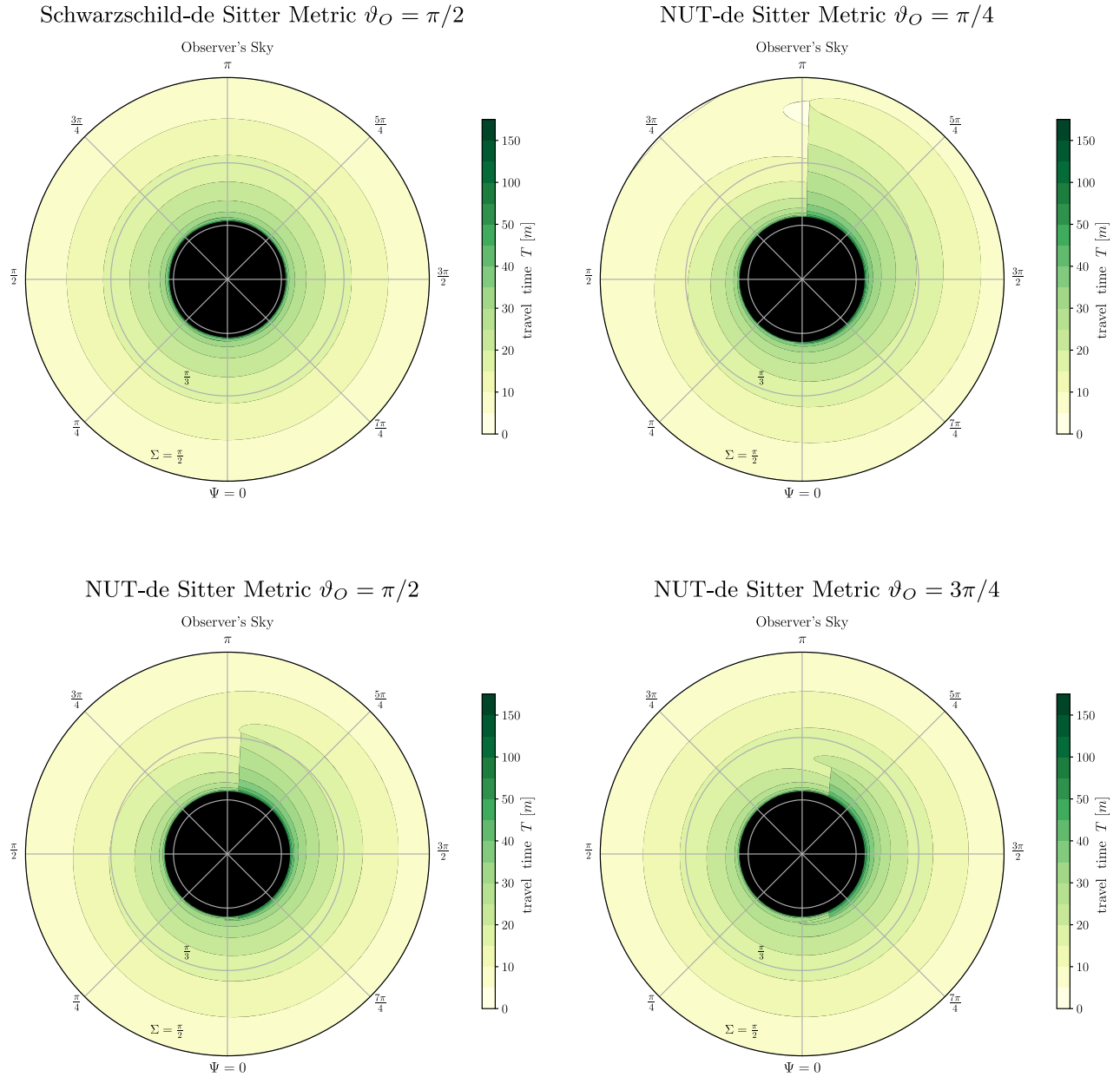


FIG. 15. Travel-time maps for light rays emitted by light sources located on the two-sphere S_L^2 at the radius coordinate $r_L = 9m$ and detected by an observer located at $r_O = 8m$ and $\vartheta_O = \pi/2$ in the Schwarzschild-de Sitter metric (top left), $\vartheta_O = \pi/4$ (top right), $\vartheta_O = \pi/2$ (bottom left), and $\vartheta_O = 3\pi/4$ (bottom right) in the NUT-de Sitter metric with $n = m/2$. The cosmological constant is $\Lambda = 1/(200m^2)$. The Misner string is located at $\vartheta = 0$ ($C = 1$).

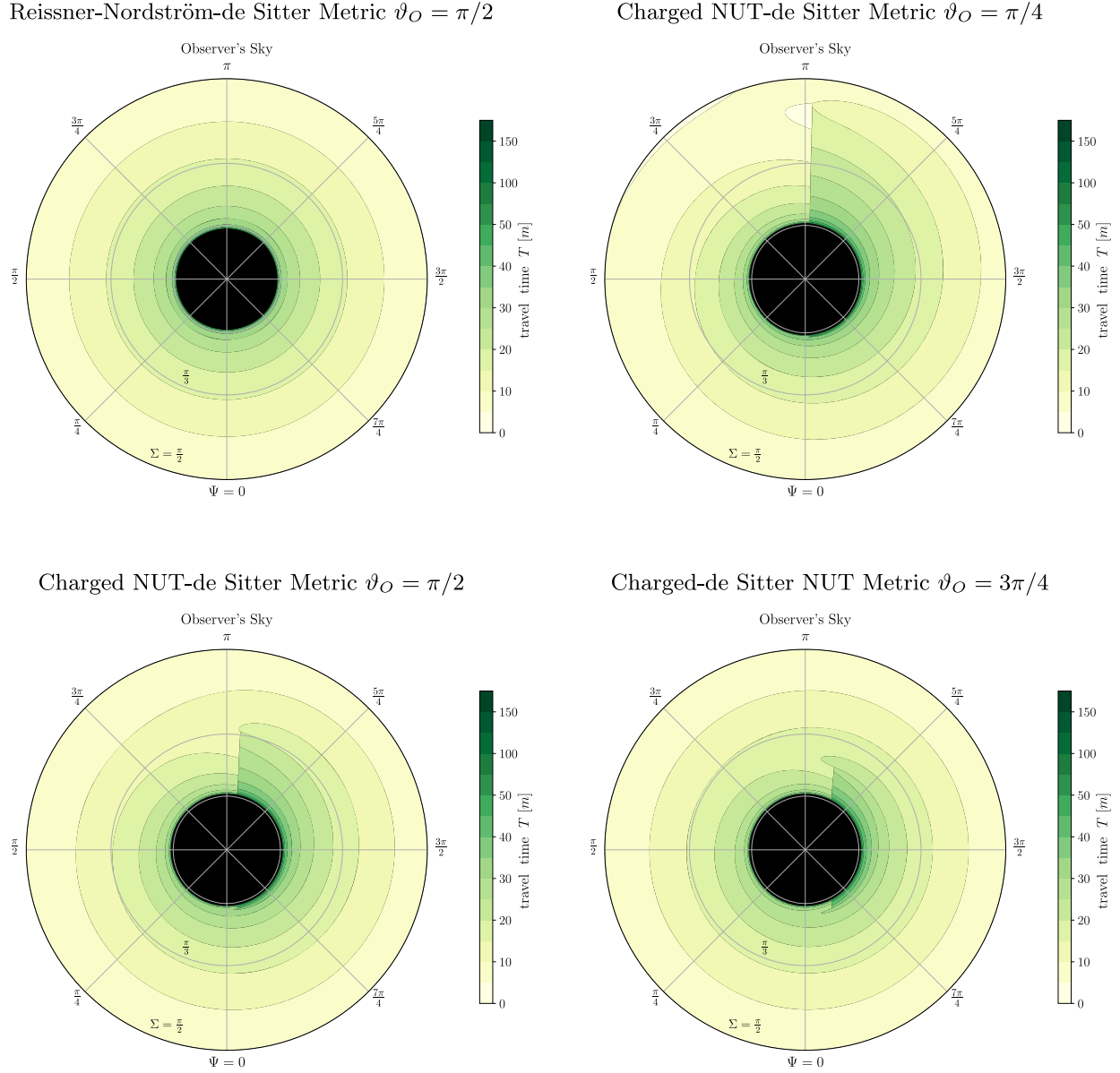


FIG. 16. Travel-time maps for light rays emitted by light sources located on the two-sphere S_L^2 at the radius coordinate $r_L = 9m$ and detected by an observer located at $r_O = 8m$ and $\vartheta_O = \pi/2$ in the Reissner-Nordström-de Sitter metric (top left), $\vartheta_O = \pi/4$ (top right), $\vartheta_O = \pi/2$ (bottom left), and $\vartheta_O = 3\pi/4$ (bottom right) in the charged NUT-de Sitter metric with $n = m/2$. The cosmological constant and the electric charge are $\Lambda = 1/(200m^2)$ and $e = 3m/4$, respectively. The Misner string is located at $\vartheta = 0$ ($C = 1$).

V. SUMMARY AND CONCLUSIONS

In this paper we first discussed and solved the equations of motion in the domain of outer communication of the charged NUT-de Sitter metrics using Legendre’s canonical forms of the elliptic integrals and Jacobi’s elliptic functions. While for ϑ and φ our results are not particularly new we believe that our representation makes them easily accessible without any further rescalings; see, e.g., Kagramanova *et al.* [14], or conventions using Killing vector fields, see, e.g., Clément *et al.* [15]. It is true that we can also use Weierstrass’ elliptic \wp function and Weierstrass’ ζ and σ

functions to solve the equations of motion for r and t ; see Kagramanova *et al.* [14]. However, using Legendre’s canonical form of the elliptic integrals has the clear advantage that we do not have to consider and manually adjust the branches of the \ln that occur in the equations for t in Kagramanova *et al.* [14]. Along the way we also derived and discussed the properties of the photon sphere and the *individual photon cones*. The radius coordinate of the photon sphere in the NUT metric was already well known for quite some time; see Jefremov and Perlick [40]. For the charged NUT-de Sitter metrics it is also included as special

case in the results of Grenzebach *et al.* [31]. However, we believe that the approach to derive it using the potential $V_r(r)$ makes it particularly easy to access and to understand the related classification of the different types of lightlike geodesic motion.

In the second part of the paper we employed the derived solutions to the equations of motion to thoroughly investigate gravitational lensing in the charged NUT–de Sitter spacetimes. For this purpose we introduced a stationary observer at the radius coordinate r_O and a two-sphere S_L^2 of light sources at the radius coordinate r_L , both measured in units of m , in the domain of outer communication between photon sphere and infinity ($\Lambda = 0$) or the cosmological horizon ($0 < \Lambda < \Lambda_C$). We introduced an orthonormal tetrad to parametrize the constants of motion using latitude-longitude coordinates on the observer’s celestial sphere following the approach of Grenzebach *et al.* [39]. In this parametrization we derived the angular radius of the shadow, set up a lens equation, defined the redshift, and the travel time.

For the charged NUT–de Sitter metrics we found that the shadow is always circular. Although the charged NUT–de Sitter metrics are only axisymmetric this result is not really surprising because the spatial component of the metrics maintains a rotational $SO(3, \mathbb{R})$ symmetry. The angular radius of the shadow is a function of the gravitomagnetic charge n and, for a fixed r_O , grows when we increase the gravitomagnetic charge. Unfortunately, as long as we do not know r_O , Λ and e , for the latter two the shadow shrinks compared to the NUT metric as soon as we turn them on, we have a degeneracy with respect to Λ , e , n and also r_O .

As first main result of this paper we wrote down an exact lens equation for the charged NUT–de Sitter metrics. Here, we have to stress that we did not derive it using numerical ray tracing but the exact analytic solutions to the equations of motion. The lens map shows images up to fourth order. We found that unlike in static and spherically symmetric spacetimes the images of first and second orders from the same quadrant on the two-sphere S_L^2 connect and are twisted. In addition we found two regions with images of first order. The first region appears relatively far away from the shadow while the second region appears very close to the shadow. In the second region the direction of the φ motion reverses and thus lightlike geodesics do not perform a full orbit about the axes $\vartheta = 0$ or $\vartheta = \pi$. The images of first and second order are separated by very clean-cut lines which mark lightlike geodesics crossing the axes. We found that for these geodesics all three spatial coordinates are regular confirming the results of Clément *et al.* [15]. In addition we found that when we turn on the cosmological constant Λ and the electric charge e the lens map maintains its basic structure.

We also discussed the potential location of the critical curves. We argued that it is unlikely that the boundaries between images of different orders from the same region on

the two-sphere S_L^2 are part of the critical curves because they immediately occur when we turn on the gravitomagnetic charge. We came to the conclusion that it is very likely that the critical curves still form circles because (i) the spacetime maintains the spatial rotational symmetry of the static and spherically symmetric spacetimes and (ii) the boundary between images of first and second order and images of third and fourth order are still circles. However, for confirming our claims and for finding the exact position of the critical curves we need a much more detailed and thorough investigation of lightlike geodesic motion in the charged NUT–de Sitter metrics, in particular the Jacobian of the lens equation, which was beyond the scope of this paper.

We also derived the redshift and plotted it as function of n for observer constellations $r_O < r_L$ and $r_L < r_O$. For the former we mainly observed blueshifts while for the latter we mainly observed redshifts. We found that for these observers the observed blueshift and the observed redshift of light rays emitted by a light source located at r_L increase with growing gravitomagnetic charge n , respectively. Adding the electric charge has only a very small effect while adding the cosmological constant Λ shifts the limits $z \rightarrow -1$ and $z \rightarrow \infty$ to much lower n .

As the second main result of this paper we derived the travel time $T(\Sigma, \Psi)$ and plotted it as a function of Σ and Ψ on the observer’s celestial sphere. When we compared the travel-time maps of the charged NUT–de Sitter metrics to their spherically symmetric and static counterparts two very distinct differences immediately caught our eye. First, for the charged NUT–de Sitter metrics the travel time shows a discontinuity when light rays cross the Misner string at least once (in our case we have $C = 1$ and thus it is located at $\vartheta = 0$). In addition, when we go from the first crossing in clockwise direction along a constant latitude Σ the travel time decreases, resulting in a spiral pattern. In addition we found that turning on the electric charge e did not significantly affect the travel time. However, in the presence of a positive cosmological constant the travel time gets significantly longer.

From the astrophysical point of view it is unfortunate that the shadow and the redshift factor z are degenerate with respect to Λ , e , n , r_O , and r_L (the latter is only true for the redshift factor z). However, the lens equation and the travel time very beautifully demonstrate that the presence of a gravitomagnetic charge is always connected with a twist in the lens map and a discontinuity in the travel time. The former was already observed in the weak-field limit by Nouri-Zonoz and Lynden-Bell [16,26] and our results confirm it for the exact lens map. The discontinuity in the travel time, and as a consequence of the time coordinate, confirms Misner’s conclusion that the time coordinate has a singularity at the Misner string [5].

The twist and the discontinuity of the travel time are unique features caused by the gravitomagnetic charge n and

therefore if they are observed for a black hole they will be strong indicators for the presence of a gravitomagnetic charge. In addition the strength of the twist and the discontinuity will also allow to draw conclusions on the magnitude of the gravitomagnetic charge n . However, for lifting the degeneracy with respect to the cosmological constant Λ , the electric charge e , the distances between observer and black hole and light source and black hole, r_O and r_L , we have to combine observations of the angular radius of the shadow, the redshift, the positions of multiple images of the same light source on the observer's celestial sphere and the travel-time differences between these images.

ACKNOWLEDGMENTS

I would like to thank Volker Perlick for the helpful discussions. I acknowledge financial support from the Cluster of Excellence QuantumFrontiers. I also acknowledge support from Deutsche Forschungsgemeinschaft within the Research Training Group 1620 Models of Gravity. I also would like to express my gratitude to all contributors to the JULIA project and in particular the authors of the packages ELLIPTIC, BLOSC, HDF5 and PYPLOT.

APPENDIX A: ELEMENTARY AND ELLIPTIC INTEGRALS

While integrating the equations of motion for r in Sec. III A and the time coordinate t in Sec. III D we encountered several elementary and elliptic integrals. In this appendix we will demonstrate how to calculate them.

1. Elementary Integrals

We start with the elementary integrals required to calculate the solutions for $r(\lambda)$ in Sec. III A 3 and the r -dependent part $t_r(\lambda)$ of the time coordinate t in Sec. III D 2 for cases 3 and 5.

a. r motion and time coordinate t : Case 3

In Secs. III A 3 and III D 2 we encountered in total five different elementary integrals associated with the geodesic motion of light rays with $E^2/K = V_r(r_{\text{ph}-})$. These geodesics have a double root at $r_1 = r_2 = r_{\text{ph}-}$ and a pair of complex conjugate roots at $r_3 = \bar{r}_4 = R_3 + iR_4$. The first two integrals I_1 and I_2 are given by Eqs. (A1) and (A2) and are easy to calculate:

$$I_1 = \int \frac{rdr}{\sqrt{(R_3 - r)^2 + R_4^2}} = \sqrt{(R_3 - r)^2 + R_4^2} + R_3 \operatorname{arsinh}\left(\frac{r - R_3}{R_4}\right), \quad (\text{A1})$$

$$I_2 = \int \frac{dr}{\sqrt{(R_3 - r)^2 + R_4^2}} = \operatorname{arsinh}\left(\frac{r - R_3}{R_4}\right). \quad (\text{A2})$$

The other three integrals I_3 , I_4 and I_5 are given by Eqs. (A3)–(A5). In I_3 and I_4 we always have $a < r$. Here a can take the values r_1 , r_{C-} , $r_{H,i}$ or $r_{H,o}$. In I_5 on the other hand we only have $a = r_{C+}$ and thus $r < a$. Now we substitute $x = r - a$ in I_3 and I_4 and $x = a - r$ in I_5 and integrate. After integration and resubstitution I_3 , I_4 and I_5 read

$$I_3 = \int \frac{dr}{(r - a)\sqrt{(R_3 - r)^2 + R_4^2}} = -\frac{1}{\sqrt{(R_3 - a)^2 + R_4^2}} \times \operatorname{arsinh}\left(\frac{(a - R_3)(r - a) + (R_3 - a)^2 + R_4^2}{(r - a)R_4}\right), \quad (\text{A3})$$

$$I_4 = \int \frac{dr}{(r - a)^2\sqrt{(R_3 - r)^2 + R_4^2}} = -\frac{\sqrt{(R_3 - r)^2 + R_4^2}}{((R_3 - a)^2 + R_4^2)(r - a)} + \frac{a - R_3}{((R_3 - a)^2 + R_4^2)^{3/2}} \times \operatorname{arsinh}\left(\frac{(a - R_3)(r - a) + (R_3 - a)^2 + R_4^2}{(r - a)R_4}\right), \quad (\text{A4})$$

$$I_5 = \int \frac{dr}{(a - r)\sqrt{(R_3 - r)^2 + R_4^2}} = \frac{1}{\sqrt{(R_3 - a)^2 + R_4^2}} \times \operatorname{arsinh}\left(\frac{(R_3 - a)^2 + R_4^2 - (a - R_3)(a - r)}{(a - r)R_4}\right). \quad (\text{A5})$$

b. r motion and time coordinate t : Case 5

In addition to the five integrals discussed in the last subsection of this appendix in Sec. III A 3 and Sec. III D 2 we also encountered four elementary integrals associated with lightlike geodesics asymptotically coming from or going to the photon sphere. In their most general form these integrals are given by $I_6 - I_9$ [Eqs. (A6)–(A9)]. In I_6 and I_7 we always have $y > a$, where a is either y_{ph} , y_{C-} , y_{C+} or $a_{2,r}/12$. y_{ph} , y_{C-} and y_{C+} are related to r_{ph} , r_{C-} and r_{C+} via Eq. (34), respectively. Now we substitute $z = y - a$ and integrate. After integration and resubstitution I_6 and I_7 read

$$I_6 = \int \frac{dy}{(y - a)\sqrt{y - y_1}} = -\frac{2}{\sqrt{a - y_1}} \operatorname{arcoth}\left(\sqrt{\frac{y - y_1}{a - y_1}}\right), \quad (\text{A6})$$

$$I_7 = \int \frac{dy}{(y - a)^2\sqrt{y - y_1}} = -\frac{\sqrt{y - y_1}}{(a - y_1)(y - a)} + \frac{1}{(a - y_1)^{3/2}} \operatorname{arcoth}\left(\sqrt{\frac{y - y_1}{a - y_1}}\right). \quad (\text{A7})$$

In I_8 and I_9 we always have $y < a$, where a is either y_{ph} , $y_{H,i}$ or $y_{H,o}$. y_{ph} , $y_{H,i}$, and $y_{H,o}$ are related to r_{ph} , $r_{H,i}$ and $r_{H,o}$ via Eq. (34), respectively. Now we substitute $z = y - y_1$

and integrate. After integration and resubstitution I_8 and I_9 read

$$I_8 = \int \frac{dy}{(a-y)\sqrt{y-y_1}} = \frac{2}{\sqrt{a-y_1}} \operatorname{artanh}\left(\sqrt{\frac{y-y_1}{a-y_1}}\right), \quad (\text{A8})$$

$$I_9 = \int \frac{dy}{(a-y)^2\sqrt{y-y_1}} = \frac{\sqrt{y-y_1}}{(a-y_1)(a-y)} + \frac{1}{(a-y_1)^{\frac{3}{2}}} \operatorname{artanh}\left(\sqrt{\frac{y-y_1}{a-y_1}}\right). \quad (\text{A9})$$

2. Elliptic Integrals

In Sec. III D 2 we encountered several general elliptic integrals. The main purpose of this section is to demonstrate how to rewrite them in terms of elementary functions and Legendre's canonical forms of the elliptic integrals of the first, second and third kind. Let us start by defining Legendre's elliptic integrals of the first, second and third kind. In their canonical form they read

$$F_L(\chi, k) = \int_0^\chi \frac{d\chi'}{\sqrt{1-k\sin^2\chi'}}, \quad (\text{A10})$$

$$E_L(\chi, k) = \int_0^\chi \sqrt{1-k\sin^2\chi'} d\chi', \quad (\text{A11})$$

$$\Pi_L(\chi, k, n_i) = \int_0^\chi \frac{d\chi'}{(1-n_i\sin^2\chi')\sqrt{1-k\sin^2\chi'}}, \quad (\text{A12})$$

where χ is called the argument of the elliptic functions, k is the square of the elliptic modulus and $n_i \in \mathbb{R}$ is an arbitrary parameter. In the case $\chi = \pi/2$ we refer to them as complete elliptic integrals. For the complete elliptic integrals one commonly omits χ in the arguments and writes the complete elliptic integral of the first kind as $K_L(k)$. The integrand of Eq. (A12) becomes singular whenever we integrate over a horizon. We can alleviate this problem by rewriting it as [56]

$$\begin{aligned} \Pi_L(\chi, k, n_i) &= F_L(\chi, k) - \Pi_L\left(\chi, k, \frac{k}{n_i}\right) \\ &+ \frac{1}{2p} \ln\left(\frac{\cos\chi\sqrt{1-k\sin^2\chi} + p\sin\chi}{|\cos\chi\sqrt{1-k\sin^2\chi} - p\sin\chi|}\right), \end{aligned} \quad (\text{A13})$$

where

$$p = \sqrt{\frac{(n_i-1)(n_i-k)}{n_i}}. \quad (\text{A14})$$

While integrating the radial part of the time coordinate $t_r(\lambda)$ in Sec. III D 2 we also encountered in total five elliptic

integrals that do not immediately take one of Legendre's canonical forms given by Eqs. (A10)–(A12). In the following we demonstrate how to rewrite them as elementary functions and Legendre's elliptic integrals of the first, second and third kind.

a. Time coordinate t : Case 2

In this case we have two pairs of complex conjugate roots. Employing the notation from Sec. III A 2 we write them as $r_1 = \bar{r}_2 = R_1 + iR_2$ and $r_3 = \bar{r}_4 = R_3 + iR_4$, where $R_1 < R_3$, $0 < R_2$, and $0 < R_4$. In this notation the integrals take the following two general forms:

$$t_{r,1}(r_i, r) = \int_{r_i}^r \frac{r'^{m_k} dr'}{\sqrt{((R_1 - r')^2 + R_2^2)((R_3 - r')^2 + R_4^2)}}, \quad (\text{A15})$$

$$\begin{aligned} t_{r,2}(r_i, r) &= \int_{r_i}^r \frac{dr'}{(r' - r_h)^{m_k} \sqrt{((R_1 - r')^2 + R_2^2)((R_3 - r')^2 + R_4^2)}}, \end{aligned} \quad (\text{A16})$$

where in our case r_h always corresponds to the radius coordinate of one of the horizons. Applying the coordinate transformation Eq. (18) and defining two new constants of motion following Byrd and Friedman [43]

$$n_1 = \frac{R_2 + g_0 R_1}{R_1 - g_0 R_2} \quad \text{and} \quad n_2 = \frac{R_2 + g_0(R_1 - r_h)}{R_1 - g_0 R_2 - r_h} \quad (\text{A17})$$

then transforms the integrals Eqs. (A15) and (A16) to

$$\begin{aligned} t_{r,1}(r_i, r) &= \frac{2(R_1 - g_0 R_2)^{m_k}}{(S + \bar{S})g_0^{m_k}} \sum_{j=0}^{m_k} \frac{m_k! n_1^{m_k-j} (g_0 - n_1)^j}{(m_k - j)! j!} \\ &\times \int_{\chi_i}^\chi \frac{d\chi'}{(1 + g_0 \tan\chi')^j \sqrt{1 - k_1 \sin^2\chi'}}, \end{aligned} \quad (\text{A18})$$

$$\begin{aligned} t_{r,2}(r_i, r) &= \frac{2}{(S + \bar{S})(R_2 + g_0(R_1 - r_h))^{m_k}} \\ &\times \sum_{j=0}^{m_k} \frac{m_k! g_0^{m_k-j} (n_2 - g_0)^j}{(m_k - j)! j!} \\ &\times \int_{\chi_i}^\chi \frac{d\chi'}{(1 + n_2 \tan\chi')^j \sqrt{1 - k_1 \sin^2\chi'}}, \end{aligned} \quad (\text{A19})$$

where S , \bar{S} , and g_0 are defined by Eqs. (16), (17), and (19), respectively, the square of the elliptic modulus k_1 is given by Eq. (23) and χ_i and χ are related to r_i and r by Eq. (22), respectively. Equations (A18) and (A19) contain elliptic integrals that do not immediately take one of Legendre's canonical forms. Thus they have to be calculated

separately. In our case we always have either $m_k = 0$, $m_k = 1$ or $m_k = 2$. For $m_k = 0$ Eqs. (A18) and (A19) reduce to the same term containing two elliptic integrals of the first kind. It is related to the Mino parameter λ by

$$\lambda - \lambda_i = \frac{i_{r_i} 2(F_L(\chi, k_1) - F_L(\chi_i, k_1))}{(S + \bar{S})\sqrt{E^2 + \frac{\Lambda}{3}K}}. \quad (\text{A20})$$

For $m_k = 1$ and $m_k = 2$ Eqs. (A18) and (A19) contain two elliptic integrals not immediately taking one of Legendre's canonical forms. The two integrals have $j = 1$ and $j = 2$ and read in their most general form

$$G_L(\chi_i, \chi, k_1, n_k) = \int_{\chi_i}^{\chi} \frac{d\chi'}{(1 + n_k \tan \chi')\sqrt{1 - k_1 \sin^2 \chi'}}, \quad (\text{A21})$$

and

$$H_L(\chi_i, \chi, k_1, n_k) = \int_{\chi_i}^{\chi} \frac{d\chi'}{(1 + n_k \tan \chi')^2 \sqrt{1 - k_1 \sin^2 \chi'}}, \quad (\text{A22})$$

where $n_k = g_0$ or $n_k = n_2$. For brevity we will now drop χ_i in the argument. Following Gralla and Lupsasca [37] we can now rewrite $G_L(\chi, k_1, n_k)$ and $H_L(\chi, k_1, n_k)$ in terms of elementary functions and Legendre's elliptic integrals of the first, second and third kind

$$G_L(\chi, k_1, n_k) = \frac{F_L(\chi, k_1) + n_k^2 \Pi_L(\chi, k_1, 1 + n_k^2)}{1 + n_k^2} + \frac{n_k \tilde{G}_L(\chi, k_1, n_k)}{2\sqrt{(1 + n_k^2)(1 - k_1 + n_k^2)}}, \quad (\text{A23})$$

$$H_L(\chi, k_1, n_k) = \frac{F_L(\chi, k_1)}{(1 + n_k^2)^2} + \frac{n_k^2}{(1 + n_k^2)(1 - k_1 + n_k^2)} \left(n_k + \frac{\sin \chi - n_k \cos \chi}{\cos \chi + n_k \sin \chi} \sqrt{1 - k_1 \sin^2 \chi} - E_L(\chi, k_1) \right) + \frac{2(1 - k_1 + n_k^2) - n_k^2 k_1}{(1 + n_k^2)(1 - k_1 + n_k^2)} \left(\frac{n_k^2 \Pi_L(\chi, k_1, 1 + n_k^2)}{1 + n_k^2} + \frac{n_k \tilde{G}_L(\chi, k_1, n_k)}{2\sqrt{(1 + n_k^2)(1 - k_1 + n_k^2)}} \right), \quad (\text{A24})$$

where

$$\tilde{G}_L(\chi, k_1, n_k) = \ln \left(\frac{\left(1 + \sqrt{\frac{1+n_k^2}{1-k_1+n_k^2}} \right) \left(1 - \sqrt{\frac{1+n_k^2}{1-k_1+n_k^2}} \sqrt{1 - k_1 \sin^2 \chi} \right)}{\left(1 - \sqrt{\frac{1+n_k^2}{1-k_1+n_k^2}} \right) \left(1 + \sqrt{\frac{1+n_k^2}{1-k_1+n_k^2}} \sqrt{1 - k_1 \sin^2 \chi} \right)} \right). \quad (\text{A25})$$

In addition, because we always have $0 < n_k^2$, we evoke Eq. (A13) to avoid the divergence of $\Pi_L(\chi, k_1, 1 + n_k^2)$.

b. Time coordinate t : Case 4

In Sec. III D 2 we also encountered the two elliptic integrals $I_L(\chi_i, \chi, k_2, n_k)$ and $J_L(\chi_i, \chi, k_2, n_k)$ that do not immediately take one of Legendre's canonical forms [k_2 is the square of the elliptic modulus given by Eq. (32) and χ_i and χ are related to r_i and r by Eq. (31), respectively]. We will now demonstrate how to rewrite them in terms of elementary functions and Legendre's elliptic integrals of the first, second and third kind. For this purpose let us first write them down in their general forms:

$$I_L(\chi_i, \chi, k_2, n_k) = \int_{\chi_i}^{\chi} \frac{d\chi'}{(1 + n_k \cos \chi')\sqrt{1 - k_2 \sin^2 \chi'}}, \quad (\text{A26})$$

$$J_L(\chi_i, \chi, k_2, n_k) = \int_{\chi_i}^{\chi} \frac{d\chi'}{(1 + n_k \cos \chi')^2 \sqrt{1 - k_2 \sin^2 \chi'}}. \quad (\text{A27})$$

We start by integrating $I_L(\chi_i, \chi, k_2, n_k)$. For this purpose we first omit, for brevity, χ_i in the argument and then expand by $1 - n_k \cos \chi'$:

$$I_L(\chi, k_2, n_k) = \int_0^{\chi} \frac{d\chi'}{(1 + n_k \cos \chi')\sqrt{1 - k_2 \sin^2 \chi'}} = \frac{1}{1 - n_k^2} \left(\int_0^{\chi} \frac{d\chi'}{\left(1 - \frac{n_k^2}{n_k^2 - 1} \sin^2 \chi' \right) \sqrt{1 - k_2 \sin^2 \chi'}} - n_k \int_0^{\chi} \frac{\cos \chi' d\chi'}{\left(1 - \frac{n_k^2}{n_k^2 - 1} \sin^2 \chi' \right) \sqrt{1 - k_2 \sin^2 \chi'}} \right). \quad (\text{A28})$$

Now we rewrite the first term as Legendre's elliptic integral of the third kind. The second term is an elementary integral. Its calculation involves several case-by-case analyses which are too long to be reproduced here. After the integration $I_L(\chi, k_2, n_k)$ becomes [38] [see also Eqs. (B61), (B62) and (B65) in Gralla and Lupsasca [37] for an alternative formulation]

$$I_L(\chi, k_2, n_k) = \frac{\Pi_L\left(\chi, k_2, \frac{n_k^2}{n_k^2-1}\right)}{1-n_k^2} + \frac{n_k \tilde{I}_L(\chi, k_2, n_k)}{2\sqrt{(n_k^2-1)(n_k^2(1-k_2)+k_2)}}, \quad (\text{A29})$$

where

$$\tilde{I}_L(\chi, k_2, n_k) = \ln \left(\frac{\sin \chi \sqrt{\frac{n_k^2(1-k_2)+k_2}{n_k^2-1}} + \sqrt{1-k_2 \sin^2 \chi}}{\left| \sin \chi \sqrt{\frac{n_k^2(1-k_2)+k_2}{n_k^2-1}} - \sqrt{1-k_2 \sin^2 \chi} \right|} \right). \quad (\text{A30})$$

For $J_L(\chi_i, \chi, k_2, n_k)$ we proceed analogously. We first omit χ_i in the argument and then expand by $(1-n_k \cos \chi')^2$ and write the third term as Legendre's elliptic integral of the third kind:

$$J_L(\chi, k_2, n_k) = \int_0^\chi \frac{d\chi'}{(1+n_k \cos \chi')^2 \sqrt{1-k_2 \sin^2 \chi'}} = \frac{2}{(n_k^2-1)^2} \left(\int_0^\chi \frac{d\chi'}{\left(1-\frac{n_k^2}{n_k^2-1} \sin^2 \chi'\right)^2 \sqrt{1-k_2 \sin^2 \chi'}} - n_k \int_0^\chi \frac{\cos \chi' d\chi'}{\left(1-\frac{n_k^2}{n_k^2-1} \sin^2 \chi'\right)^2 \sqrt{1-k_2 \sin^2 \chi'}} \right) + \frac{\Pi_L\left(\chi, k_2, \frac{n_k^2}{n_k^2-1}\right)}{n_k^2-1}. \quad (\text{A31})$$

The first term is again an elliptic integral. It is given by Eq. (A34) in Sec. A 2 c and its evaluation will be discussed there. The second term is, again, an elementary integral. Together their evaluation requires several case-by-case analyses. After the integration and simplifying all terms $J_L(\chi, k_2, n_k)$ reads [see also Eqs. (B61)–(B65) in Gralla and Lupsasca [37] for an alternative formulation]

$$J_L(\chi, k_2, n_k) = \frac{n_k^3 \sin \chi \sqrt{1-k_2 \sin^2 \chi}}{(n_k^2-1)(n_k^2(1-k_2)+k_2)(1+n_k \cos \chi)} - \frac{n_k(n_k^2(1-2k_2)+2k_2)\tilde{I}_L(\chi, k_2, n_k)}{2((n_k^2-1)(n_k^2(1-k_2)+k_2))^{\frac{3}{2}}} + \frac{F_L(\chi, k_2)}{n_k^2-1} - \frac{n_k^2 E_L(\chi, k_2)}{(n_k^2-1)(n_k^2(1-k_2)+k_2)} + \frac{(n_k^2(1-2k_2)+2k_2)\Pi_L\left(\chi, k_2, \frac{n_k^2}{n_k^2-1}\right)}{(n_k^2-1)^2(n_k^2(1-k_2)+k_2)}. \quad (\text{A32})$$

Note that in $I_L(\chi, k_2, n_k)$ and $J_L(\chi, k_2, n_k)$ we always have $n_k^2/(n_k^2-1) > 1$ and thus we again evoke Eq. (A13) to avoid the divergence of $\Pi_L(\chi, k_2, n_k^2/(n_k^2-1))$.

c. Time coordinate t : Case 6

In Sec. III D 2 and Appendix A 2 b we encountered the elliptic integral $M_L(\chi_i, \chi, k_i, n_k)$ in two different forms [$k_i = k_2$ or $k_i = k_3$ is the square of the elliptic modulus given by Eqs. (32) or (46) and χ_i and χ are related to r_i and r by Eqs. (31), (45) or (49), respectively]. In its explicit form it reads

$$M_L(\chi_i, \chi, k_i, n_k) = \int_{\chi_i}^\chi \frac{d\chi'}{(1-n_k \sin^2 \chi')^2 \sqrt{1-k_i \sin^2 \chi'}}. \quad (\text{A33})$$

We can now rewrite this integral in terms of elementary functions and Legendre's elliptic integrals of the first, second and third kind (again we omit the first argument χ_i):

$$M_L(\chi, k_i, n_k) = \int_0^\chi \frac{d\chi'}{(1-n_k \sin^2 \chi')^2 \sqrt{1-k_i \sin^2 \chi'}} = \frac{n_k^2 \sin(2\chi) \sqrt{1-k_i \sin^2 \chi}}{4(n_k-k_i)(n_k-1)(1-n_k \sin^2 \chi)} + \frac{F_L(\chi, k_i)}{2(n_k-1)} - \frac{n_k E_L(\chi, k_i)}{2(n_k-k_i)(n_k-1)} + \frac{n_k(n_k-2) - (2n_k-3)k_i}{2(n_k-k_i)(n_k-1)} \Pi_L(\chi, k_i, n_k). \quad (\text{A34})$$

Note that for the integral in Sec. A 2 b we have to replace $n_k \rightarrow n_k^2/(n_k^2-1)$. For lightlike geodesics with turning

points at $r_{\min} = r_1$ and $r_{\max} = r_2$ we always chose the coordinate transformations Eq. (42) and Eq. (47) such that Legendre's elliptic integral of the third kind does not diverge. Therefore, in these two cases we can use Eq. (A34) directly.

APPENDIX B: ELLIPTIC FUNCTIONS

In this appendix we demonstrate how to solve the differential equation associated with the equation of motion for r given by Eq. (6) for case 2, case 4 and case 6 in Sec. III A 3 using Jacobi's elliptic functions. Before we turn to explicitly solving the differential equation we will give a brief introduction to Jacobi's elliptic functions and their properties. For a thorough introduction we refer the interested reader to the book of Hancock [44].

The theory of elliptic functions after Jacobi defines three elementary elliptic functions. These are Jacobi's sn, cn and dn functions. Starting from the sine and the cosine they are defined by

$$\operatorname{sn}(\lambda, k) = \sin \operatorname{am} \lambda = \sin \chi, \quad (\text{B1})$$

$$\operatorname{cn}(\lambda, k) = \cos \operatorname{am} \lambda = \cos \chi, \quad (\text{B2})$$

$$\operatorname{dn}(\lambda, k) = \sqrt{1 - k \sin^2 \operatorname{am} \lambda} = \sqrt{1 - k \sin^2 \chi}, \quad (\text{B3})$$

where for now λ is an arbitrary independent variable, k is the square of the elliptic modulus and $\chi = \operatorname{am} \lambda$ is called the amplitude of λ . In addition one can also define six associated elliptic functions. In this paper we only need one, Jacobi's elliptic sc function. It is defined by

$$\operatorname{sc}(\lambda, k) = \frac{\operatorname{sn}(\lambda, k)}{\operatorname{cn}(\lambda, k)}. \quad (\text{B4})$$

Jacobi's elliptic functions are periodic with respect to the complete elliptic integral of the first kind $K_L(k)$ and fulfill the following periodicity relations:

$$\operatorname{sn}(\lambda \pm 4K_L(k), k) = \operatorname{sn}(\lambda, k), \quad (\text{B5})$$

$$\operatorname{cn}(\lambda \pm 4K_L(k), k) = \operatorname{cn}(\lambda, k), \quad (\text{B6})$$

$$\operatorname{dn}(\lambda \pm 2K_L(k), k) = \operatorname{dn}(\lambda, k), \quad (\text{B7})$$

$$\operatorname{sc}(\lambda \pm 2K_L(k), k) = \operatorname{sc}(\lambda, k). \quad (\text{B8})$$

Jacobi's elliptic functions have the characteristic that they solve the differential equation

$$\left(\frac{d\chi}{d\lambda}\right)^2 = a(1 - k \sin^2 \chi). \quad (\text{B9})$$

Although Eq. (6) does not immediately take the Legendre form of Eq. (B9), using an appropriate coordinate transformation $z = f(\sin \chi)$, $z = f(\cos \chi)$ or $z = f(\tan \chi)$ we can transform any differential equation of the form

$$\left(\frac{dz}{d\lambda}\right)^2 = a_4 z^4 + a_3 z^3 + a_2 z^2 + a_1 z + a_0 \quad (\text{B10})$$

into the form of Eq. (B9). Now we separate variables and integrate:

$$\int_{\lambda_i}^{\lambda} d\lambda' = \frac{i_{\chi_i}}{\sqrt{a}} \int_{\chi_i}^{\chi} \frac{d\chi'}{\sqrt{1 - k \sin^2 \chi'}}, \quad (\text{B11})$$

where $1/\sqrt{a} = c/\sqrt{a_4}$, $i_{\chi_i} = \operatorname{sgn}(d\chi/d\lambda|_{\chi=\chi_i})$ and c is a new constant that is specific to the chosen coordinate transformation. We can now rewrite this equation as

$$\tilde{\lambda} = i_{\chi_i} \frac{\sqrt{a_4}}{c} (\lambda - \lambda_i) + F_L(\chi_i, k) = \int_0^{\chi} \frac{d\chi'}{\sqrt{1 - k \sin^2 \chi'}}. \quad (\text{B12})$$

With $\chi = \operatorname{am} \tilde{\lambda}$ we can now write the solution $z(\lambda)$ to Eq. (B9) in terms of Jacobi's elliptic sn, cn, and sc functions.

-
- [1] J. F. Plebanski and M. Demianski, Rotating, charged, and uniformly accelerating mass in general relativity, *Ann. Phys. (N.Y.)* **98**, 98 (1976).
 [2] V. S. Manko and E. Ruiz, Physical interpretation of the NUT family of solutions, *Classical Quantum Gravity* **22**, 3555 (2005).
 [3] A. H. Taub, Empty space-times admitting a three parameter group of motions, *Ann. Math.* **53**, 472 (1951).

- [4] E. Newman, L. Tamburino, and T. Unti, Empty-space generalization of the Schwarzschild metric, *J. Math. Phys. (N.Y.)* **4**, 915 (1963).
 [5] C. W. Misner, The flatter regions of Newman, Unti, and Tamburino's generalized Schwarzschild space, *J. Math. Phys. (N.Y.)* **4**, 924 (1963).
 [6] W. B. Bonnor, A new interpretation of the NUT metric in general relativity, *Proc. Cambridge Philos. Soc.* **66**, 145 (1969).

- [7] A. Sackfield, Physical interpretation of N.U.T. metric, *Proc. Cambridge Philos. Soc.* **70**, 89 (1971).
- [8] J. B. Griffiths and J. Podolský, *Exact Space-Times in Einstein's General Relativity* (Cambridge University Press, Cambridge, England, 2009), pp. 213–237.
- [9] D. R. Brill, Electromagnetic fields in a homogeneous, and nonisotropic universe, *Phys. Rev.* **133**, B845 (1964).
- [10] G. Clément, D. Gal'tsov, and M. Guenouche, NUT wormholes, *Phys. Rev. D* **93**, 024048 (2016).
- [11] V. A. Ruban, Non-singular metrics of Taub-Newman-Unti-Tamburino type with an electromagnetic field, *Dokl. Akad. Nauk SSSR* **204**, 1086 (1972), http://www.mathnet.ru/php/archive.phtml?wshow=paper&jrmid=dan&aperid=36957&option_lang=eng.
- [12] C. W. Misner and A. H. Taub, A singularity-free empty universe, *Sov. Phys. JETP* **28**, 122 (1969), <https://ui.adsabs.harvard.edu/abs/1969JETP...28..122M/abstract>.
- [13] J. G. Miller, M. D. Kruskal, and B. B. Godfrey, Taub-NUT (Newman, Unti, Tamburino) metric and incompatible extensions, *Phys. Rev. D* **4**, 2945 (1971).
- [14] V. Kagramanova, J. Kunz, E. Hackmann, and C. Lämmerzahl, Analytic treatment of complete and incomplete geodesics in Taub-NUT space-times, *Phys. Rev. D* **81**, 124044 (2010).
- [15] G. Clément, D. Gal'tsov, and M. Guenouche, Rehabilitating space-times with NUTs, *Phys. Lett. B* **750**, 591 (2015).
- [16] D. Lynden-Bell and M. Nouri-Zonoz, Classical monopoles: Newton, NUT space, gravomagnetic lensing, and atomic spectra, *Rev. Mod. Phys.* **70**, 427 (1998).
- [17] S. Rahvar and M. Nouri-Zonoz, Gravitational microlensing in NUT space, *Mon. Not. R. Astron. Soc.* **338**, 926 (2003).
- [18] The LIGO Scientific Collaboration *et al.*, Advanced LIGO, *Classical Quantum Gravity* **32**, 074001 (2015).
- [19] F. Acernese *et al.*, Advanced Virgo: A second-generation interferometric gravitational wave detector, *Classical Quantum Gravity* **32**, 024001 (2015).
- [20] T. Akutsu *et al.*, Construction of KAGRA: An underground gravitational-wave observatory, *Prog. Theor. Exp. Phys.* **2018**, 013F01 (2018).
- [21] The Event Horizon Telescope Collaboration *et al.*, First M87 Event Horizon Telescope results. I. The shadow of the supermassive black hole, *Astrophys. J. Lett.* **875**, L1 (2019).
- [22] The Event Horizon Telescope Collaboration *et al.*, First M87 Event Horizon Telescope results. II. Array and instrumentation, *Astrophys. J. Lett.* **875**, L2 (2019).
- [23] N. S. Kardashev *et al.*, “RadioAstron”—A telescope with a size of 300 000 km: Main parameters and first observational results, *Astronomy Reports* **57**, 153 (2013).
- [24] N. S. Kardashev *et al.*, RadioAstron science program five years after launch: Main science results, *Solar System Research* **51**, 535 (2017).
- [25] R. L. Zimmerman and B. Y. Shahir, Geodesics for the NUT metric and gravitational monopoles, *Gen. Relativ. Gravit.* **21**, 821 (1989).
- [26] M. Nouri-Zonoz and D. Lynden-Bell, Gravomagnetic lensing by NUT space, *Mon. Not. R. Astron. Soc.* **292**, 714 (1997).
- [27] M. Halla and V. Perlick, Application of the Gauss-Bonnet theorem to lensing in the NUT metric, *Gen. Relativ. Gravit.* **52**, 112 (2020).
- [28] M. C. Werner, Gravitational lensing in the Kerr-Randers optical geometry, *Gen. Relativ. Gravit.* **44**, 3047 (2012).
- [29] S.-W. Wei, Y.-X. Liu, C.-E. Fu, and K. Yang, Strong field limit analysis of gravitational lensing in Kerr-Taub-NUT spacetime, *J. Cosmol. Astropart. Phys.* **10** (2012) 053.
- [30] M. Sharif and S. Iftikhar, Equatorial gravitational lensing by accelerating and rotating black hole with NUT parameter, *Astrophys. Space Sci.* **361**, 36 (2016).
- [31] A. Grenzebach, V. Perlick, and C. Lämmerzahl, Photon regions and shadows of Kerr-Newman-NUT black holes with a cosmological constant, *Phys. Rev. D* **89**, 124004 (2014).
- [32] A. Grenzebach, *The Shadow of Black Holes*, Springer Briefs in Physics (Springer, Cham, 2016).
- [33] A. R. Forsyth, Note on the central differential equation in the relativity theory of gravitation, *Proc. R. Soc. A* **97**, 145 (1920).
- [34] W. B. Morton, The forms of planetary orbits on the theory of relativity, *London, Edinburgh, Dublin Philos. Mag. J. Sci.* **42**, 511 (1921).
- [35] C. Darwin, The gravity field of a particle, *Proc. R. Soc. A* **249**, 180 (1959).
- [36] X. Yang and J. Wang, YNOGK: A new public code for calculating null geodesics in the Kerr spacetime, *Astrophys. J. Suppl. Ser.* **207**, 6 (2013).
- [37] S. E. Gralla and A. Lupsasca, Null geodesics of the Kerr exterior, *Phys. Rev. D* **101**, 044032 (2020).
- [38] T. C. Frost and V. Perlick, Lightlike geodesics and gravitational lensing in the spacetime of an accelerating black hole, *Classical Quantum Gravity* **38**, 085016 (2021).
- [39] A. Grenzebach, V. Perlick, and C. Lämmerzahl, Photon regions and shadows of accelerated black holes, *Int. J. Mod. Phys. D* **24**, 1542024 (2015).
- [40] P. I. Jefremov and V. Perlick, Circular motion in NUT spacetime, *Classical Quantum Gravity* **33**, 245014 (2016).
- [41] Y. Mino, Perturbative approach to an orbital evolution around a supermassive black hole, *Phys. Rev. D* **67**, 084027 (2003).
- [42] T. C. Frost, Gravitational lensing by charged accelerating black holes, [arXiv:2111.00283](https://arxiv.org/abs/2111.00283).
- [43] P. F. Byrd and M. D. Friedman, *Handbook of Elliptic Integrals for Engineers and Physicists*, 1st ed., Die Grundlehren der Mathematischen Wissenschaften (Springer-Verlag, Berlin, Heidelberg, 1954).
- [44] H. Hancock, *Elliptic Integrals*, 1st ed., edited by M. Merriman and R. S. Woodward, Mathematical Monographs (John Wiley & Sons, New York, 1917).
- [45] J. L. Synge, The escape of photons from gravitationally intense stars, *Mon. Not. R. Astron. Soc.* **131**, 463 (1966).
- [46] R. Penrose, The apparent shape of a relativistically moving sphere, *Proc. Cambridge Philos. Soc.* **55**, 137 (1959).
- [47] M. Mars, C. F. Paganini, and M. A. Oancea, The fingerprints of black holes—shadows and their degeneracies, *Classical Quantum Gravity* **35**, 025005 (2018).
- [48] S. Frittelli and E. T. Newman, Exact universal gravitational lensing equation, *Phys. Rev. D* **59**, 124001 (1999).
- [49] V. Perlick, Exact gravitational lens equation in spherically symmetric and static spacetimes, *Phys. Rev. D* **69**, 064017 (2004).

- [50] J. Bezanson, A. Edelman, S. Karpinski, and V.B. Shah, Julia: A fresh approach to numerical computing, *SIAM Rev.* **59**, 65 (2017).
- [51] A. Bohn, W. Thrope, F. Hébert, K. Henriksson, D. Bunandar, M. A. Scheel, and N. W. Taylor, What does a binary black hole merger look like?, *Classical Quantum Gravity* **32**, 065002 (2015).
- [52] N. Straumann, *General Relativity*, 2nd ed., Graduate Texts in Physics (Springer, Heidelberg, 2013).
- [53] J. Fohlmeister, C. S. Kochanek, E. E. Falco, J. Wambsganss, M. Oguri, and X. Dai, A two-year time delay for the lensed quasar SDSS J1029 + 2623, *Astrophys. J.* **764**, 186 (2013).
- [54] E. Koptelova *et al.*, Time delay between images of the lensed quasar UM673, *Astron. Astrophys.* **544**, A51 (2012).
- [55] S. H. Suyu *et al.*, H0LiCOW I. H_0 Lenses in COSMOGRAILs Wellspring: Program overview, *Mon. Not. R. Astron. Soc.* **468**, 2590 (2017).
- [56] L. M. Milne-Thomson, Elliptic integrals, in *Handbook of Mathematical Functions With Formulas, Graphs, and Mathematical Tables*, 10th ed. Applied Mathematics Series, edited by M. Abramowitz and I. A. Stegun (U. S. Dept. of Commerce, National Bureau of Standards, Washington D. C., 1972), pp. 587–607.